UNIVERSIDAD DE INVESTIGACIÓN DE TECNOLOGÍA EXPERIMENTAL YACHAY

Escuela de Ciencias Físicas y Nanotecnología

TÍTULO: Synthesis and characterization of semiconducting Zinc Oxide (ZnO) nanofibers.

Trabajo de integración curricular presentado como requisito para la obtención del título de Físico.

Autor:

Pomaquiza Castillo Sergio Israel

Tutora:

PhD. Almache Hernández Rosa

Urcuquí, Noviembre 2024

Autoría

Yo, **Sergio Israel Pomaquiza Castillo**, con cédula de identidad 0302528914, declaro que las ideas, juicios, valoraciones, interpretaciones, consultas bibliográficas, definiciones y conceptualizaciones expuestas en el presente trabajo; así cómo, los procedimientos y herramientas utilizadas en la investigación, son de absoluta responsabilidad de el/la autor/a del trabajo de integración curricular. Así mismo, me acojo a los reglamentos internos de la Universidad de Investigación de Tecnología Experimental Yachay.

Urcuquí, Noviembre 2024.

Sergio Israel Pomaquiza Castillo
CI: 0302528914

Autorización de publicación

Yo, **Sergio Israel Pomaquiza Castillo**, con cédula de identidad 0302528914, cedo a la Universidad de Investigación de Tecnología Experimental Yachay, los derechos de publicación de la presente obra, sin que deba haber un reconocimiento económico por este concepto. Declaro además que el texto del presente trabajo de titulación no podrá ser cedido a ninguna empresa editorial para su publicación u otros fines, sin contar previamente con la autorización escrita de la Universidad.

Asimismo, autorizo a la Universidad que realice la digitalización y publicación de este trabajo de integración curricular en el repositorio virtual, de conformidad a lo dispuesto en el Art. 144 de la Ley Orgánica de Educación Superior.

Urcuquí, Noviembre 2024.

Sergio Israel Pomaquiza Castillo
CI: 0302528914

Dedication

To my parents, Sergio and Miriam, and my siblings, Erika, Camila, and Mateo, for their unconditional love, support, and trust, which have been my greatest source of inspiration.
To my tutor, PhD. Rosa Almache, for her expert guidance and constant support throughout this process.
As Greg Anderson said, "The trick is to enjoy the journey and not just the destination." This thesis is a reflection of that journey full of learning and growth.
Thank you all for being part of this experience.
With gratitude and affection,

Sergio Pomaquiza.

Acknowledgment

I wish to express my sincere gratitude to all the people who have contributed to the development and completion of this thesis.

First and foremost, I want to thank my thesis advisor, PhD. Rosa Almache, for her invaluable guidance, patience, and constant support. Her expertise and suggestions have been fundamental to the realization of this project.

I also appreciate Professor Benjamín Pusay, and laboratory technicians Johanna and Fernanda, for their valuable assistance and support during the research process. Their contribution has been essential in overcoming the challenges I encountered.

My eternal gratitude goes to my parents, Sergio and Miriam, and my siblings, Erika, Camila, and Mateo, for their unconditional love, sacrifices, and constant support throughout my studies. Their faith in me has been a source of inspiration and strength.

Finally, my thanks to all those who have in some way contributed to the completion of this thesis, whether through advice, words of encouragement, or moral support. Your influence has been a great motivation.

Thank you all.

Sergio Pomaquiza.

Resumen

Este trabajo se enfocó en la fabricación de nanofibras electrohiladas a partir de una solución de alcohol polivinílico (PVA) y nitrato de zinc, para obtener nanofibras de óxido de zinc (ZnO) mediante calcinación. Se realizaron caracterizaciones estructurales, morfológicas y eléctricas utilizando espectroscopía Raman, difracción de rayos X (XRD), espectroscopía infrarroja por transformada de Fourier (FTIR), análisis termogravimétrico (TGA), microscopía electrónica de barrido (SEM), microscopía de fuerza atómica (AFM) y la función lineal potenciostática de intensidad de corriente-voltaje (C-V) del potenciostato. La espectroscopía Raman y el XRD mostraron picos característicos que confirmaron la formación de ZnO a partir de una temperatura de calcinación de 500 °C. El análisis FTIR identificó grupos funcionales y estructuras moleculares tanto de las nanofibras de PVA/nitrato de zinc como de las nanofibras de ZnO. SEM reveló que la solución al 4% es ideal para la síntesis, ya que produjo una cantidad abundante de nanofibras con diámetros más uniformes. Los análisis TGA mostraron que las nanofibras de PVA/nitrato de zinc tienen estabilidad térmica desde los 450°C, mientras que el PVA puro la tiene a partir de 500°C. El análisis AFM estimó que las nanofibras de PVA/nitrato de zinc antes de la calcinación tienen un diámetro entre 1500 y 2000 nm, que se reduce en un 90% tras la calcinación, con diámetros entre 120 y 380 nm para las nanofibras de ZnO. Las mediciones eléctricas mostraron que la resistencia calculada en sustratos FTO con nanofibras de PVA/nitrato de zinc y con nanofibras de ZnO aumenta conforme incrementa el tiempo de electrohilado.

Palabras clave:
Nanofibras electrohiladas, alcohol polivinílico, medidas eléctricas, nanofibras de óxido de zinc.

Abstract

This work focused on the fabrication of electrospun nanofibers from a solution of polyvinyl alcohol (PVA) and zinc nitrate to obtain zinc oxide (ZnO) nanofibers through calcination. Structural, morphological, and electrical characterizations were carried out using Raman spectroscopy, X-ray diffraction (XRD), Fourier transform infrared spectroscopy (FTIR), thermogravimetric analysis (TGA), scanning electron microscopy (SEM), atomic force microscopy (AFM), and the potentiostat's "Current intensity-Voltage (C-V) linear potentiostatic function". Raman spectroscopy and XRD showed characteristic peaks that confirmed the formation of ZnO starting at a calcination temperature of 500 °C. FTIR analysis identified functional groups and molecular structures of both PVA/zinc nitrate nanofibers and ZnO nanofibers. SEM revealed that the 4% solution is ideal for synthesis, as it produced a large quantity of nanofibers with more uniform diameters. TGA analysis showed that PVA/zinc nitrate nanofibers have thermal stability starting at 450 °C, while pure PVA has stability starting at 500 °C. AFM analysis estimated that the PVA/zinc nitrate nanofibers before calcination have diameters between 1500 and 2000 nm, which are reduced by 90% after calcination, with diameters between 120 and 380 nm for ZnO nanofibers. Electrical measurements showed that the calculated resistance in FTO substrates with PVA/zinc nitrate nanofibers and ZnO nanofibers increases as electrospinning time increases.

Keywords:
Electrospun nanofibers, polyvinyl alcohol, electrical measurements, zinc oxide nanofibers.

Contents

List of Figures

List of Tables

Chapter 1

Introduction

The United Nations (UN) agenda has established Sustainable Development Goals, including climate action, well-being and health, and life on land, all aimed at improving the quality of accessible resources such as air. In recent decades, increasing awareness of air quality and the need to address issues related to atmospheric pollution have driven research into advanced gas detection technologies. Among emerging materials in this field, zinc oxide (ZnO) based nanofibers have emerged as a promising platform for manufacturing highly sensitive and selective gas sensors.

Air quality has become a matter of vital importance on the UN agenda due to its direct impacts on human health and the environment[2]. The presence of atmospheric pollutants, such as volatile organic compounds (VOCs), combustion gases, and other toxic gases, poses significant risks to public health and ecosystem sustainability[2]. Accurately and efficiently monitoring these gases is essential to implement preventive actions and reduce the negative impacts of air pollution[2].

In this context, gas sensors play a crucial role by providing an essential tool for early detection and continuous monitoring of harmful gases in the air[3]. The evolution of nanotechnology has triggered significant advances in the manufacturing of sensors based on nanomaterials, harnessing the unique properties of nanomaterials to enhance the sensitivity and selectivity of gas detection devices[3].

Among these nanomaterials, ZnO-based nanofibers have emerged as an attractive option due to their exceptional properties, such as high surface area, ease of functionalization, and rapid response to changes in the gas environment[4]. Research into ZnO nanofibers for gas detection has

experienced exponential growth in recent years, driven by interest in overcoming the limitations of conventional sensors[4]. Notable advances have been made in the synthesis of ZnO nanofibers using various techniques, including electrospinning, which enables the production of nanometric diameter fibers with a desirable porous structure for gas detection applications[5].

Among these nanomaterials, ZnO-based nanofibers have emerged as an attractive option due to their exceptional properties such as high surface area, ease of functionalization, and rapid response to changes in the gas environment[4]. Research on ZnO nanofibers for gas detection has seen exponential growth in recent years, driven by interest in overcoming the limitations of conventional sensors[4]. Significant advances have been made in the synthesis of ZnO nanofibers using various techniques, including electrospinning, which enables the production of nanofibers with uniform diameters and a desirable porous structure for gas detection applications[5].

In previous studies, Park (2009) successfully fabricated ZnO nanofibers by combining the sol-gel process, mixing zinc acetate and polyvinylpyrrolidone (PVP), resulting in ZnO nanofibers with diameters ranging from 35 nm to 100 nm[6]. On the other hand, Blachowicz and Ehrmann (2020) used a solution of polyvinylpyrrolidone (PVP) and zinc nitrate[7]. After stirring the solution, it achieved an optimized viscosity suitable for electrospinning[7]. Following electrospinning, the nanofibers were collected and calcined at temperatures between 500 °C and 800 °C to remove the polymer and obtain pure ZnO nanofibers[7]. A successful process for fabricating ZnO nanofibers was also carried out by Di Mauro (2016) by combining the sol-gel process, mixing zinc acetate and polyvinylpyrrolidone (PVP)[8]. An optimized viscosity solution suitable for electrospinning was obtained[8]. After obtaining and collecting the nanofibers, they were calcined at different temperatures ranging from 350 °C to 650 °C to remove the polymer and obtain pure ZnO nanofibers with an average diameter of 50 nm[8]. Comparing these results with those obtained in this work, ZnO nanofibers with diameters ranging from 120 nm to 380 nm were achieved here. Additionally, only a calcination temperature of 500 °C was used.

This work delves into the synthesis, characterization, and morphological and electrical analysis of ZnO nanofibers, exploring their potential for future applications using Polyvinyl alcohol (PVA) and Zinc Nitrate as precursors. It aims to make significant practical contributions, paving the way for future applications in gas sensors that could be implemented in real-world settings such as environmental monitoring stations, industrial facilities, and portable devices for public health. Enhanced gas detection capabilities can have a direct impact on environmental safety and the

health of local communities.

1.1 Problem Statement

In recent decades, research in nanomaterials has grown significantly due to their unique nanoscale properties. Among these materials, zinc oxide (ZnO) nanofibers have stood out for their potential in sensitive and selective gas sensors, capable of detecting pollutants such as volatile organic compounds (VOCs) and combustion gases[9]. The electrospinning technique is effective for producing nanofibers with controlled diameters and uniform structures[10].

However, the synthesis and characterization of ZnO nanofibers from a solution of polyvinyl alcohol (PVA) and zinc nitrate pose significant challenges. The combination of these materials and their processing via the Electrospinning technique requires a profound understanding of the optimal conditions to achieve nanofibers with the desired physical and chemical properties. The main challenge lies in the uniform formation of nanofibers and in the subsequent thermal conversion to zinc oxide nanofibers without deteriorating the fibrous structure.

1.2 General and Specific Objectives

1.2.1 General Objective

- To synthesize zinc oxide nanofibers through the calcination of electrospun PVA/Zinc nitrate nanofibers.

1.2.2 Specific Objectives

- Determine the optimal concentration of the PVA/Zinc nitrate solution.

- Optimize the calcination temperature for the formation of ZnO nanofibers from the PVA/Zinc nitrate solution.

- Characterize the structural properties of the samples.

- Study the vertical resistance of the zinc oxide nanofibers through Current intensity-Voltage (C-V) measurements.

Chapter 2

Theoretical Background

2.1 Semiconductors

2.1.1 Definition, Importance and Applications

Semiconductors are materials that have electrical properties, positioned intermediate on the conductivity scale between a conductor and an insulator[11]. At very low temperatures they behave as insulators, and at high temperatures or when subjected to an external electric field, they behave as conductors[11]. These materials have a very narrow band gap compared to insulators, but wider than conductors (Figure 2.1). This gap determines the amount of energy needed to excite an electron from the valence to the conduction band, affecting their ability to conduct electricity, and they have a resistivity range between $10^{-2}\ \Omega \cdot \text{cm}$ and $10^6\ \Omega \cdot \text{cm}$[12].
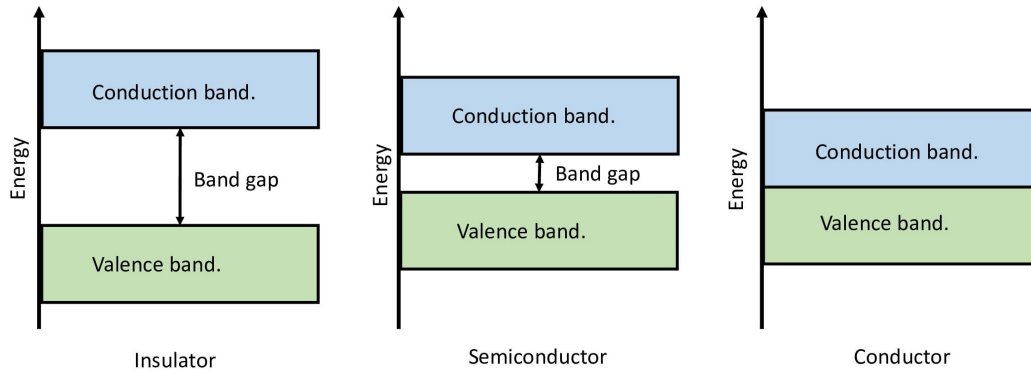
Figure 2.1: A reference diagram showing the bandgap size for a conductor, semiconductor, and insulator.

Semiconductors can be doped to alter their electrical properties[11], these semiconductors are known as extrinsic semiconductors[11]. And they are divided into:

- P-type semiconductors: These are doped with trivalent atoms such as boron, creating "holes" in the crystal structure that act as positive charge carriers[12], the introduction of these "holes" shifts the Fermi level toward the valence band[13] (Figure 2.2).

- N-type semiconductors: These are doped with pentavalent atoms such as phosphorus, which introduce additional electrons into the crystal structure, acting as negative charge carriers[14]. Due to this increase of electrons, the Fermi level shifts toward the conduction band[13] (Figure 2.2).

On the other hand, there are intrinsic semiconductors, which are pure materials without doping, in which the electrical conductivity is solely due to the thermally generated electrons and holes[14] (Figure 2.2). For example: pure silicon, pure germanium.
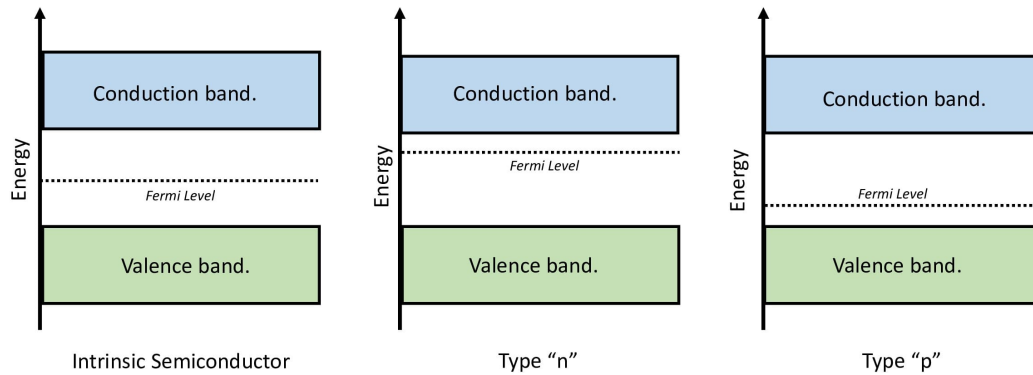
Figure 2.2: Reference diagram of the Fermi Level of extrinsic and intrinsic semiconductors.

Semiconductors are crucial today in our society for their ability to precisely and efficiently regulate the flow of current[11]. Since the creation of the transistor in 1947, semiconductors have had a revolutionary impact across a wide range of technological sectors, including computing, electronics, energy, and communications. The ongoing reduction in the size of semiconductor-based electronic components has enabled the development of more powerful and compact devices[13].

These materials play a crucial role in the nano realm, facilitating significant advances in miniaturized and efficient electronics, such as transistors and integrated circuits at microscopic scales that improve the speed and efficiency of electronic devices[15]. Additionally, semiconductors are employed to develop precise sensors that detect gases, liquids, and biomolecules, useful in medical, environmental, and security applications. In renewable energy, nanostructured semiconductors are transforming the solar industry with high-efficiency, low-cost cells[16]. On the other hand, advanced materials like carbon nanotubes and semiconductor-derived nanoparticles offer solutions in flexible electronics and lightweight, strong materials. For the environment, semiconductors are fundamental in advanced filters for water purification, sensors for precise environmental monitoring, and in agriculture for controlled release systems of fertilizers and pesticides, minimizing the impact on ecosystems[17]. This convergence of technologies shows how semiconductors not only drive innovation but also promote sustainable solutions for global environmental challenges.

2.1.2 Classification

Elementals

Elemental semiconductors are materials formed by a single type of atom and have properties inter-mediate between conductors and insulators[18]. The two most common elemental semiconductors are silicon (Si) and germanium (Ge). Elemental semiconductors have a band gap that allows the control of electrical conduction through the introduction of impurities (doping)[19]. Some common applications include their use in the fabrication of power control and energy management devices, as the basis for the production of microprocessors and other integrated components in electronic devices, and in the manufacturing of LEDs and lasers[20].

Compounds

Compound semiconductors consist of the combination of two or more chemical elements, usually from different groups of the periodic table[21]. These materials integrate the properties of their constituent elements, offering superior control over their electrical and optical characteristics compared to elemental semiconductors[21]. The main classifications are:

Binary Semiconductors: These are composed of two different elements[19]. They are classi-fied into:

- III-V Semiconductors: Formed by elements from group III and V of the periodic table[18], examples: Gallium arsenide (GaAs), Indium phosphide (InP), etc.

- II-VI Semiconductors: Formed by elements from group II and VI of the periodic table[18], examples: Zinc selenide (ZnSe), Cadmium sulfide (CdS), etc.

- IV-IV Semiconductors: Formed by elements from group IV of the periodic table[18], exam-ple: Silicon carbide (SiC), etc.

- Transition Metal Oxides (TMO): Transition metal oxides are an important class of semi-conductors. These are composed of a transition metal and oxygen[22], examples: Zinc oxide (ZnO), Titanium dioxide (TiO_2), etc.

Ternary Semiconductors: These are composed of three different elements[18]. They are typically derived from binary semiconductors with the addition of a third element to adjust

their properties[20], examples: AlGaAs (Aluminum gallium arsenide), InGaAs (Indium gallium arsenide), etc.

Quaternary Semiconductors: These are composed of four different elements[18]. They allow greater flexibility in adjusting the material's properties[20], examples: InGaAsP (Indium gallium arsenide phosphide), AlInGaP (Aluminum indium gallium phosphide), etc.

Some of the most common applications of compound semiconductors include their key roles in lithium-ion batteries, supercapacitors, and solar cells[22]. They are used for the creation of gas, humidity, and temperature sensors due to their properties sensitive to environmental changes, in the decomposition of organic pollutants, and for generating hydrogen from water[22].

2.2 Transition Metal Oxides (TMO)

Transition Metal Oxides (TMO) are a class of semiconductors, composed of transition metals found in groups 3 to 12 of the periodic table, and oxygen[23]. Some examples of these materials are oxides of titanium, manganese, tungsten, zinc, copper, vanadium, etc. Metal oxides can exhibit a wide range of crystal structures with electronic properties that range from insulating to semiconducting and conducting[24]. Their electronic properties can be modified by changing their morphology, doping, and stoichiometry[23]. This versatility is due to the variability in the band gap size and the ability of the metals to change their oxidation state[24].

An important point to highlight is the oxygen vacancies, which are defects in the crystal lattice of transition metal oxides where oxygen atoms are missing[25]. These defects can significantly influence the physical and chemical properties of the material. Their formation is due to:

- Thermal Treatments: Calcination at high temperatures in reducing atmospheres or under vacuum can induce the formation of oxygen vacancies[26].

- Chemical Reduction: Chemical reactions with reducing agents can create oxygen vacancies by removing oxygen atoms from the crystal lattice[27].

- Irradiation: Irradiation with high-energy particles can cause the expulsion of oxygen atoms, generating vacancies[28].

On the other hand, the impact of oxygen vacancies in TMOs acts on electrical properties as doping centers, introducing donor states within the band gap and increasing electrical conductivity[29]. In optical properties, they can induce changes such as photoluminescence, due to the creation of energy levels within the band gap[30]. Finally, these vacancies also enhance the surface reactivity of the material, improving its catalytic activity[29].

To finish, some applications of certain transition metal oxides:

- Titanium dioxide (TiO_2) is used in solar cells and as a photocatalyst. Additionally, oxygen vacancies in TiO_2 can enhance its photocatalytic activity and its ability to generate hydrogen from water[31].

- Zinc oxide (ZnO) is used in sensors and optoelectronic devices due to its piezoelectric and photoconductive properties. Furthermore, oxygen vacancies in ZnO are responsible for visible light emission and enhancing sensitivity in gas sensors[32].

- Copper oxide (CuO and Cu_2O) is employed in solar cells and as a catalyst.

- Iron oxide (Fe_2O_3) and manganese oxide (MnO_2) are used to remove water contaminants through adsorption and oxidation processes.

2.2.1   Zinc Oxide (ZnO)

Zinc oxide (ZnO) is one of the most studied metal oxides due to its wide range of applications in fields such as photovoltaics, sensing, optoelectronics, and piezoelectricity[33]. This compound is a type "n" binary semiconductor with a direct band gap of approximately 3.3 eV at room temperature[23]. The significant electronegativity difference between zinc and oxygen imparts a high degree of ionicity to its bonding, making it one of the most ionic compounds[23]. This high ionicity results in strong charge repulsion, stabilizing its most stable crystalline structure in a hexagonal form known as the wurtzite type structure[34]. The work function of ZnO, which is the energy required to release an electron from its surface, varies with crystal orientation and surface preparation, and is typically found between 4.3 and 5.3 eV[34] (Figure 2.3).
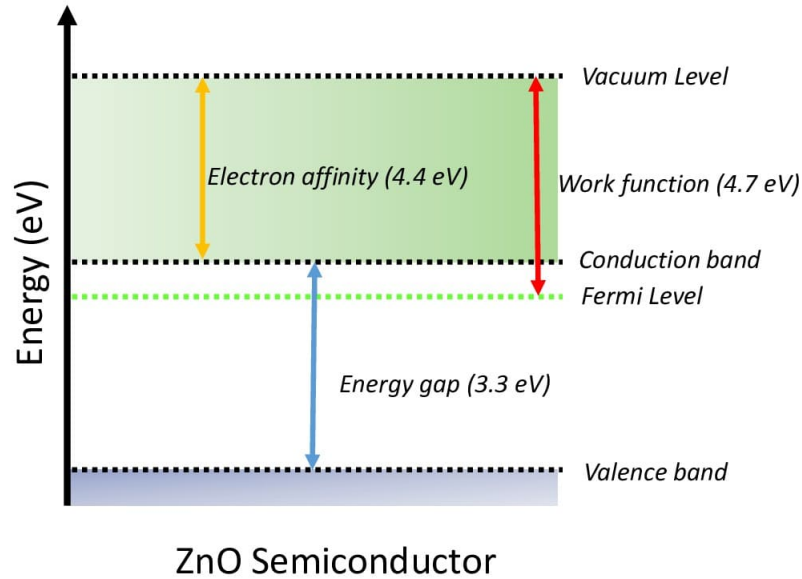
Figure 2.3: Schematic diagram of ZnO bands[1].

On the other hand, vacancies in Zinc Oxide (ZnO) are divided: Oxygen vacancies are common defects in ZnO and act as donors, introducing free electrons into the conduction band[35]. Zinc vacancies are less common than oxygen vacancies and tend to act as acceptors, affecting the band structure and optical properties[36]. The impact of oxygen vacancies increases electrical conductivity by acting as donors and providing free electrons to the conduction band[37]. Finally, vacancies affect the photoluminescence of ZnO, influencing visible and ultraviolet light emission, which is crucial for optoelectronic applications[38].

Some applications of Zinc Oxide (ZnO) include its use in the manufacture of ultraviolet LEDs and in gas sensors due to its high sensitivity and selectivity in detecting gases such as NO_2, O_2, and H_2[34]. It is employed in biosensors for detecting biomolecules due to its biocompatibility[39]. ZnO is also used as a photocatalyst in the treatment of wastewater to degrade organic contaminants such as dyes and pharmaceuticals[40]. Lastly, ZnO is effective in the photocatalysis of volatile organic compounds (VOCs) and other toxic chemicals present in air and water, contributing to environmental purification[41].

2.3 Nanofibers

Nanofibres are fibres with diameters that are generally found within a range of nanometers. These can be produced from different polymers, and from there they obtain different physical properties and functional capabilities, to generate important applications. There are many methods for synthesizing nanofibers, but the most common ones are:

- **Electrospinning**: A method that uses an electrical field to extrude dissolved polymers into solvents, creating aligned nanofibres with diameters ranging from nanometers to micrometers, useful in biomedical applications, filters and composite materials[42].

- **Self-assembly**: A method in which molecules or nanoparticles are spontaneously organized into ordered structures using intermolecular or interfacial interactions to create nanofibers that have distinctive characteristics in biomaterials and electronic devices[42].

- **Thermal induction separation phase**: Method in which phases are separated into a polymeric solution while cooling or drying. This creates nanofibers using controlled temperature changes to create fibrillary structures in membrane and composite materials[42].

Some more common applications about nanofibers:

- Nanofibers are used as three-dimensional matrices for cell growth and differentiation. An example of this is regeneration of bone and cartilage tissues[43].

- Due to their high retention and capture efficiency, nanofibers are used in water filters to effectively remove contaminants and pathogens[44].

- In textiles, the incorporation of nanofibers can provide features such as water resistance, self-cleaning and temperature control[45].

- In flexible electronic devices, such as sensors and flexible displays, nanofibers are used as conductive and dielectric components[46].

- Due to their high surface area and porosity, nanofibers are used as catalyst supports, which increases catalyst efficiency and reduces the use of precious metals[47].

2.4   Zinc Oxide Nanofibers

Zinc oxide (ZnO) nanofibers are very interesting due to their special properties, including high electrical conductivity, exceptional optical properties, and photocatalytic activity. Park successfully fabricated ZnO nanofibers by combining the sol-gel process, mixing zinc acetate and polyvinylpyrrolidone (PVP), and then stirring for 3 hours at 70 °C until a homogeneous solution was obtained[6]. Finally, a solution with an optimized viscosity suitable for Electrospinning was obtained. After obtaining and collecting the nanofibers, they were calcined from 400 to 800 °C for 1 hour to remove the polymer. Finally, the diameters of the obtained nanofibers ranged from 35 nm to 100 nm, and the activation energy of the ZnO nanofibers was inversely proportional to the annealing temperature[6].

On the other hand, Blachowicz and Ehrmann used a solution of polyvinylpyrrolidone (PVP) and zinc nitrate, after stirring the solution, it obtained an optimized viscosity for electrospinning. After electrospinning, the nanofibers were collected and calcined at temperatures from 500 to 800 °C to remove the polymer and obtain pure ZnO nanofibers[7].

Siddheswaran successfully fabricated ZnO nanofibers by combining the sol-gel process, mixing zinc acetate and polyvinyl alcohol (PVA), then stirring for 1 hour, and then maintaining it in a constant temperature bath at 50 °C for 6 hours for the reaction to proceed[48]. Finally, a solution with an optimized viscosity suitable for Electrospinning was obtained. After obtaining and collecting the nanofibers, they were dried at 60 °C under vacuum for 8 hours and calcined at different temperatures from 400 to 800 °C to remove the polymer and obtain pure ZnO nanofibers[48].

Finally, a successful process of fabricating ZnO nanofibers was carried out by Di Mauro by combining the sol-gel process, mixing zinc acetate and polyvinylpyrrolidone (PVP), and preparing 2 different solutions with concentrations of 10 and 15 % to observe the effect of concentration on the electrospinning process[8]. Finally, a solution with an optimized viscosity suitable for Electrospinning was obtained. After obtaining and collecting the nanofibers, they were calcined at different temperatures from 350 to 650 °C to remove the polymer and obtain pure ZnO nanofibers with an average diameter of 50 nm[8].

2.5   Manufacturing Techniques

2.5.1   Electrospinning

Electrospinning technique

Electrospinning is a technique used for the formation of polymer fibers that requires an electric field to produce fibers ranging from 2 nm to several micrometers in diameter. Both natural and synthetic polymers are used to produce nanofibers[49]. In the electrospinning technique, a direct current voltage in the kilovolt range is required between the needle and a collector (a surface that will collect the fibers), creating a strong electric field[42]. Under the influence of the electric field, the surface of the solution at the tip of the needle deforms to form a conical structure known as a "Taylor cone"[42]. If the intensity of the electric field is sufficient, the surface tension of the solution is overcome, and a fine jet of this solution is expelled from the tip of the Taylor cone. As the solution jet moves towards the collector, it stretches and thins due to electrostatic forces and the evaporation of the solvent (or cooling in the case of melted polymers)[42]. This process can generate very thin and continuous fibers. The resulting fibers are deposited randomly or in specific patterns on the collector, depending on the equipment design and the collection process[42].

2.5.2   Calcination Process

Calcination Technique

Muffle calcination is a specific technique within the general calcination process, in which a muffle furnace is used to perform the thermal decomposition of compounds at high temperatures. In this technique, the material to be calcined is first placed in a crucible suitable for withstanding high temperatures[50]. The muffle furnace is programmed to reach and maintain the desired temperature, and the heating and cooling ramps can be adjusted according to the material's needs. The material is then kept at the calcination temperature for a specific time to ensure complete decomposition or reaction[50]. Finally, once the calcination time is completed, the furnace is cooled in a controlled manner to avoid thermal shocks and obtain the desired material[50].

2.6   Characterization Techniques

2.6.1   Raman spectroscopy

Raman spectroscopy is an analytical technique used to investigate vibrations, rotations, and low-frequency transitions in molecules through the inelastic scattering of light[51]. When a laser beam hits a sample, most photons are scattered elastically, but a very small fraction undergoes an energy change due to interactions with the vibrational modes of the molecules, a phenomenon known as Raman scattering[52]. This energy change causes a shift in the frequency of the scattered light, generating a characteristic spectrum. This spectrum provides detailed information about the chemical bonds and molecular structure, making it particularly useful for identifying compounds and analyzing their structural properties[53]. Additionally, Raman spectroscopy allows for the analysis of samples in solid, liquid, or gaseous states without requiring special preparation, making it an ideal tool for applications in chemistry, biology, materials science, and nanotechnology[51].

2.6.2   X-Ray Diffraction (XRD)

X-ray diffraction (XRD) is a crucial analytical technique for analyzing the crystalline structure of materials. When a beam of X-rays strikes a crystal, the atoms in the crystal act as a diffraction grating, deflecting the X-rays at specific angles depending on the internal atomic arrangement of the crystal[54]. This phenomenon is described by Bragg's law ($n\lambda = 2d \sin \theta$), where n is the diffraction order, λ is the wavelength of the X-rays, d is the distance between crystal planes, and θ is the angle of incidence[55]. The diffraction pattern obtained is captured with a detector and analyzed with specialized software to reconstruct the three-dimensional structure of the crystal, allowing for the determination of key parameters such as the unit cell constant, symmetry, and atomic positions[56]. This technique is essential in diverse fields such as chemistry, materials physics, and structural biology, where it is used to identify mineral phases, examine mechanical and thermal properties of materials, and elucidate the structure of biological macromolecules[55].

2.6.3   Scanning electron microscopy (SEM)

The Scanning Electron Microscope (SEM) is an advanced instrument that uses an electron beam to create high-resolution images of the surface of samples[57]. Electrons, generated by a filament

and accelerated by a high voltage, interact with the atoms of the sample, producing signals such as secondary electrons (SE), backscattered electrons (BSE), and characteristic X-rays[58]. These signals are detected and converted into detailed images that show the topography, structure, and elemental composition of the sample[59]. SEM is fundamental in materials research, surface analysis, and elemental microanalysis of a variety of materials, from metals and polymers to biomaterials and biological tissues[57].

2.6.4 Thermogravimetric Analysis (TGA)

Thermogravimetric Analysis (TGA) is a technique that measures the mass variation of a sample as it is heated, cooled, or maintained at a constant temperature in a controlled environment[60]. The sample is placed in a small container within an oven, where it undergoes a temperature program while a microbalance records the mass changes relative to temperature[61]. These mass changes, caused by phenomena such as decomposition, oxidation, dehydration, and gas release, are represented in a TGA curve[62]. This curve allows for the determination of thermal stability, composition, and decomposition temperature of materials. TGA is essential for the characterization of polymers, organic and inorganic compounds, and for determining the purity and thermal stability of various materials[61].

2.6.5 Atomic Force Microscope (AFM)

Atomic Force Microscopy is a high-resolution technique used to observe and analyze surfaces at the nanometric scale[63]. It operates by using a probe with an extremely fine tip that moves over the sample, interacting with van der Waals, electrostatic, and contact forces[64]. These interactions cause deflections in a cantilever, which are measured with a laser and a photodetector, generating a detailed map of the surface topography[63]. AFM can operate in various modes, including contact, non-contact, and tapping, allowing for precise visualization of atomic structures and measurement of mechanical and chemical properties. It is essential in fields such as nanomechanics and cellular biology.

2.6.6   Fourier Transform Infrared Spectroscopy (FTIR)

Fourier Transform Infrared Spectroscopy (FTIR) is an analytical technique used to identify compounds and study the molecular structure of materials through the absorption of infrared radiation[65]. This radiation causes characteristic molecular vibrations, and absorption frequencies are specific to different chemical bonds and functional groups[66]. The resulting spectrum provides a unique "fingerprint" of the substance, enabling both qualitative and quantitative identification of organic and inorganic compounds[65]. In FTIR, infrared radiation passes through the sample, and an interferometer breaks down the signal into frequency components[67]. A Fourier transform then converts the data into a spectrum that relates absorbance or transmittance to the wavenumber (cm^{-1}), typically in the range of 400-4000 cm^{-1}. It is widely used in fields like chemistry, biomedicine, and materials science to characterize plastics, biomolecules, polymers, and other materials[66].

Chapter 3

Methodology

3.1   Reagents

Polyvinyl alcohol (*PVA*) (Mw = 130000 $\frac{g}{mol}$), Zinc nitrate ($Zn(NO_3)_2$) (Mw = 297.49 $\frac{g}{mol}$), and Zinc oxide (*ZnO*) (Mw = 81.39 $\frac{g}{mol}$, pH = 6.72, purity = 99.99 %) from Sigma and Aldrich Co.

3.2   Preparation of 11% *PVA* solution

Polyvinyl alcohol was prepared with 14.3 g of PVA mixed in 130 mL of distilled water. This was stirred at 685 rpm for 3 hours at 90°C until a homogeneous solution with an 11% w/v concentration was obtained (Figure 3.1).
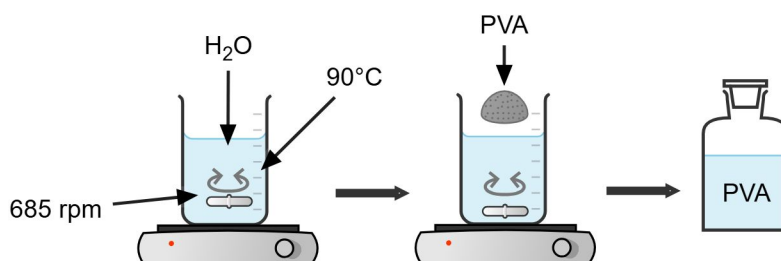
Figure 3.1: Schematic representation of the preparation of 11% PVA.

3.3 Preparation of 11% *PVA* + 10% *Zn(NO$_3$)$_2$* solution

For the preparation of this solution, 9 g of Zinc Nitrate were dissolved in 10 mL of distilled water, and this was then mixed with 90 mL of 11% PVA. This mixture was stirred for 2 hours at 685 rpm at 70°C, and a viscous solution of PVA/Zinc Nitrate was obtained to find an ideal ratio between 11% *PVA* and 10% *Zn(NO$_3$)$_2$*. This solution was used to analyze the formation of zinc oxide (ZnO) using the calcination technique at different temperatures ranging from 200 to 1000°C.

3.4 Preparation of 11% *PVA* + 2%, 4% and 6% *Zn(NO$_3$)$_2$* solutions

For the preparation of these 3 solutions, 0.2, 0.4, and 0.6 g of zinc nitrate were dissolved in 10 mL of distilled water for each amount. These 3 zinc nitrate solutions were each mixed with 9.8, 9.6, and 9.4 mL of 11% PVA, respectively. These solutions were stirred for 2 hours at 685 rpm at 70°C, and viscous solutions of PVA/zinc nitrate were obtained to find an ideal ratio between 11% *PVA* and *Zn(NO$_3$)$_2$* (Figure 3.2). Additionally, the pH of each solution was measured to ensure it was not lower than 5.5 or higher than 7, to avoid damage to the electrospinning metal needle in the future. Table 3.1 shows how each solution was prepared at different concentrations of Zn(NO$_3$)$_2$.
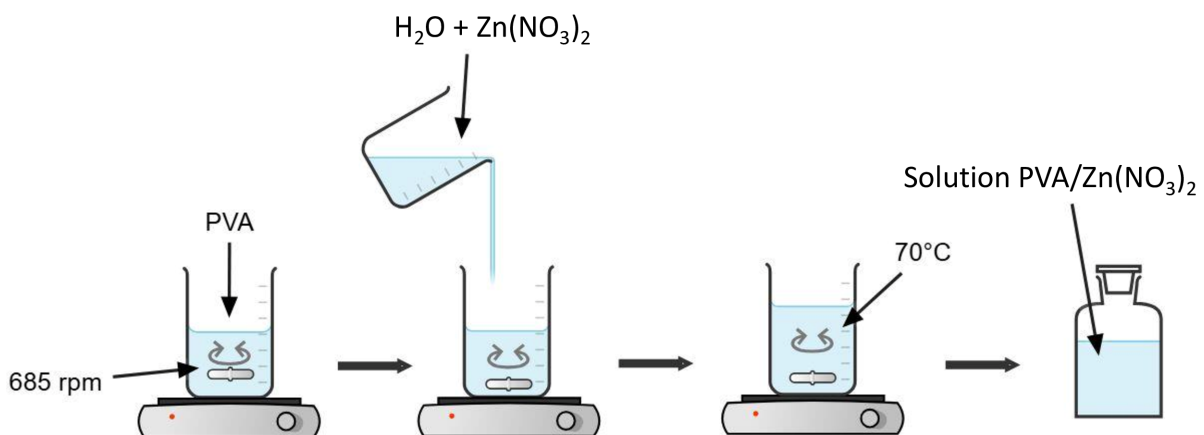
Figure 3.2: Schematic representation of the preparation of the $PVA/Zn(NO_3)_2$ solution.

Solution name	PVA volume (ml)	H_2O volume (ml)	Amount of $Zn(NO_3)_2$ (g)	pH	Final concentration of PVA (w/v)	Final concentration of $Zn(NO_3)_2$ (w/v)
2% solution	9.8	10	0.2	5.89	5.44%	1.01%
4% solution	9.6	10	0.4	5.81	5.39%	2.04%
6% solution	9.4	10	0.6	5.57	5.33%	3.09%

Table 3.1: Preparation of each solution at different initial concentrations of $Zn(NO_3)_2$: 2%, 4%, and 6% with 11% PVA.

3.5 Synthesis of nanofibers

3.5.1 Electrospinning

Equipment and Procedure

For this thesis, the SprayBaseTM electrospinning equipment available in the Biology laboratory of Yachay Tech University was used to manufacture the nanofibers. This equipment allows controlling and monitoring all the parameters involved in the electrospinning process: voltage, height, flow, temperature, and pressure (Figure 3.3 (a), (b) and (c)). Additionally, the equipment has a camera and a light source that allows us to observe the drop and monitor the formation of the Taylor cone.
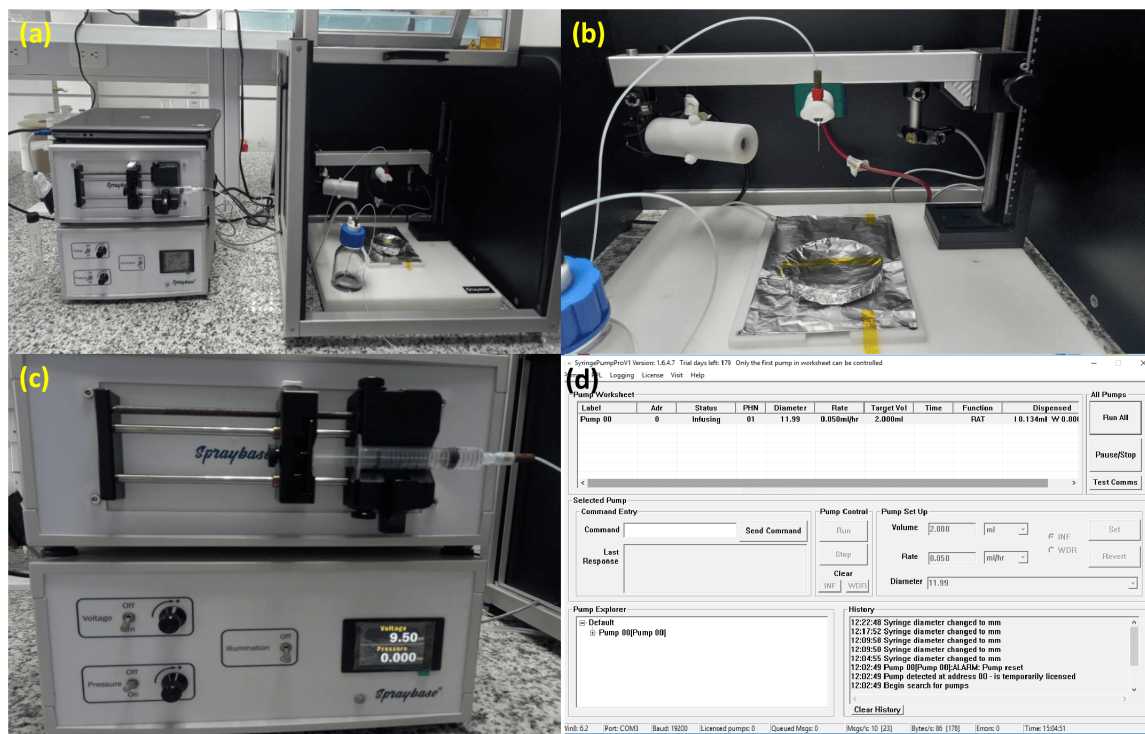
Figure 3.3: (a) Electrospinning equipment, (b) Zoom of the right side of the Electrospinning, (c) Zoom of the left side of the Electrospinning, and (d) SyringePumpProV1 software interface

On the other hand, each solution must have an adequate viscosity. After that, a volume of the solution is placed in the syringe, the probe is connected, and the solution is made to flow through it. Then the needle is connected, and the solution is also made to flow through it. Once this is done, the needle is placed in the cathode, the anode is covered with aluminum foil, and the appropriate height between the needle and the collector is adjusted. We then proceed to turn on the equipment, where the SyringePumpProV1 software (Figure 3.3 (d)) will be used to control the flow and diameter, in addition to being able to pause the electrospinning process. We then turn on the camera and the light source, which will allow us to observe the drop and monitor the formation of the Taylor cone. Finally, we turn on and vary the voltage until finding the appropriate one that gives us the formation of nanofibers. Table 3.2 shows the parameters at which nanofibers were obtained for each solution.

Solution name	2% solution	4% solution	6% solution
Voltage	8.5 – 9.5 kV	9.5 kV	9 - 9.5 kV
Flow	50 µL/h	20 µL/h	0.90 µL/h
Height	12 cm		
Syringe diameter	1.44 cm		
Needle diameter	0.09 cm		
Temperature	19 °C		
Volume put into the syringe	3000 µL		

Table 3.2: Parameters of nanofiber formation at different concentrations of $Zn(NO_3)_2$ and 11 % PVA.

3.5.2   Calcination Process

Equipment and Procedure

For this thesis, the BOECO 8/1100 muffle furnace available in the Physics Laboratory at Yachay Tech University was used to calcine the nanofibers and the PVA/zinc nitrate solution. This equipment allows control and monitoring of the parameters involved in the calcination process: temperature, ramp, and time. Nine calcination processes were carried out using the PVA/zinc nitrate solution in the muffle furnace. In each calcination process was used 10 mL of the solution,

placed in a rectangular crucible. This solution contained 11% PVA and 10% zinc nitrate. The only parameter varied in each calcination process was the temperature, which ranged from 200 to 1000 °C. The ramp rate was 10 °C/min and the calcination time was 6 hours; these two parameters were kept constant. Additionally, each nanofiber sample obtained was placed on a silicon substrate and calcined at 500 °C with a ramp of 10 °C/min for 6 hours to obtain the nanofibers required for this thesis (Figure 3.4).
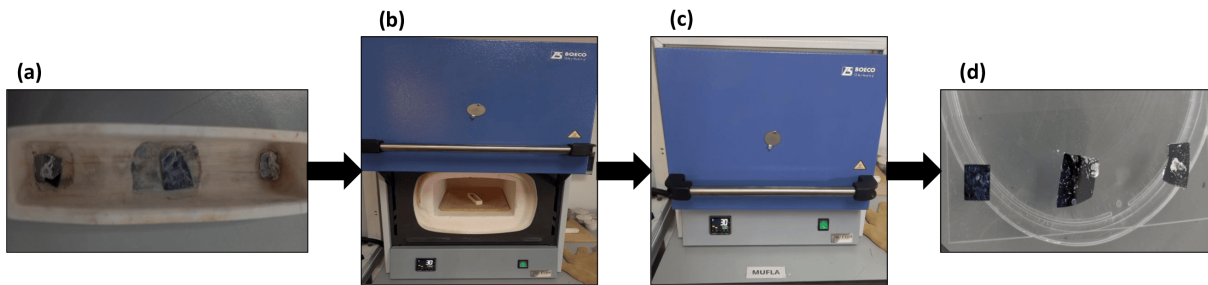
Figure 3.4: Schematic representation of the calcination process: (a) Placing nanofibers on a silicon substrate, (b) Inserting the sample into the muffle, (c) Closing and setting the parameters required for calcining, and (d) ZnO nanofibers.

3.6 Characterization of nanofibers

3.6.1 Raman spectroscopy

For this thesis was used the LabRAM HR Evolution Raman spectroscopy equipment (Figure 3.5) available in the Physics Laboratory at Yachay Tech University, noted for its high resolution and versatility. This equipment covers a wide range of wavelengths and allows configuration for different types of samples, including solid, liquid, and gaseous. Its confocal technology and high-sensitivity detectors facilitate obtaining Raman images with high spatial resolution, ideal for analyzing complex structures at the microscopic level. Equipped with intuitive software and automation functions, the LabRAM HR Evolution is suitable for a wide range of applications in nanotechnology, biology, chemistry, and environmental sciences, offering detailed data for the

characterization of materials, compound identification, and analysis of chemical and biological processes.

Figure 3.5: Raman spectrometer.

A Raman spectroscopy analysis was performed on powder obtained from the calcination at different temperatures of the 11% PVA and 10% Zinc Nitrate solution. A laser with a wavelength of 633 nm and 100% power was used. The acquisition time was set at 15 seconds with 15 accumulations per measurement. The Raman wavenumber range was set between 20 and 2000 cm^{-1}. A x50 objective was used for the microscopy of the powders. The instrument's grating was set to 600.

3.6.2   X-Ray Diffraction (XRD)

For this thesis was used a X-ray Diffractometer for polycrystalline samples (Figure 3.6), Brand Rigaku, model Miniflex 600, equipped with a 600W X-ray tube, Bragg-Brentano goniometer with an 8-position automatic sampler, D/tex Ultra detector, and SmartLab Studio II software, available in the Chemistry laboratory at Yachay Tech University.

Figure 3.6: X-ray Diffractometer.

A X-ray diffraction analysis was performed on powder obtained from the calcination at different temperatures of the 11% PVA and 10% Zinc Nitrate solution. An X-ray generator was operated at 40 kV and 15 mA, with CuK(alpha) radiation source (sealed tube). For data collection, a $\theta/2\theta$ scan axis was used, with a step width of 0.01°, scan range of 20° to 80° in 2θ, at a speed of 10°/min, and D/tex Ultra2 detector in 1D scan mode.

3.6.3 Thermogravimetric Analysis (TGA)

For this thesis was used a Thermogravimetric Analyzer (Figure 3.7), brand TA Instruments, model TGA 55, equipped with an automatic loader, furnace (Pt/Rh), dual gas inlet manifold (N_2 and Air), operational temperature range from room temperature to 1000°C, controlled linear heating rate modes (from 0.1 to 100°C/min) or ballistic heating rate mode (>600°C/min), platinum and alumina sample pans with a maximum capacity of 1000 mg and a resolution of 0.1 µg, available in the Chemistry laboratory at Yachay Tech University.

Figure 3.7: Thermogravimetric Analyzer.

A Thermogravimetric Analysis was performed on *PVA*/$Zn(NO_3)_2$ nanofibers obtained from the electrospinning of 4% solution. The following parameters were used: heating ramp from room temperature to 900°C, heating rate of 10°C/min, air atmosphere, and a 100 µL platinum crucible.

3.6.4 Atomic Force Microscope (AFM)

For this thesis was used an Atomic Force Microscope (AFM) from Park Systems (Figure 3.8), available at the Physics Laboratory of Yachay Tech University. This equipment is designed for surface characterization at the nanometric scale. Its key components include a cantilever with a sharp PPP-NCHR tip, a piezoelectric scanner for precise movements, a laser detection system to measure deflections, and advanced software for control and analysis.

Figure 3.8: Atomic Force Microscope.

An Atomic Force Microscopy analysis was performed on the non-calcined and calcined nanofibers obtained from the 4% solution via electrospinning. The following parameters were used: a cantilever with a sharp PPP-NCHR tip, non-contact mode, and a frequency of 0.19 Hz for non-calcined nanofibers and 0.42 Hz for calcined nanofibers.

3.6.5 Fourier Transform Infrared Spectroscopy (FTIR)

For this thesis was used an Agilent Cary 630 FTIR spectrometer (Figure 3.9) available at the Biology Laboratory of Yachay Tech University. It operates with a 25 mm Michelson interferometer and covers a broad spectral range depending on the crystal: KBr (6300-350 cm^{-1}) and ZnSe (5100-600 cm^{-1}). The resolution is better than 2 cm^{-1}. The wavenumber precision and reproducibility are notable, with values of 0.05 cm^{-1} and 0.005 cm^{-1}, respectively, according to ASTM 1921 standards. It also supports techniques such as diamond ATR, diffuse reflectance, and transmission.

Figure 3.9: FTIR spectrometer.

FTIR analysis was performed on $PVA/Zn(NO_3)_2$ nanofibers obtained from a 4% solution, and also on ZnO nanofibers obtained from the calcination of $PVA/Zn(NO_3)_2$ nanofibers. The following parameters were used: Default mode, KBr crystal, spectral range from 400 to 4000 cm^{-1}, background scans of 32, sample scans of 32, resolution of 4 cm^{-1}, and a threshold of 0.002.

3.6.6 Current Intensity-Voltage (C-V) linear potentiostatic function in the Potentiostat

The Current intensity-Voltage (C-V) linear potentiostatic function involves using a potentiostat to apply a controlled voltage sweep between a working electrode and a reference electrode[68]. During this process, the current flowing through the electrochemical system is measured, providing detailed information about the electrode's response and the electrochemical reactions taking place[68].

For this thesis was used a potentiostat device, Metrohm Autolab brand, model VIONIC powered by INTELLO, available in the Physics laboratory at Yachay Tech University. This

equipment is capable of maintaining and controlling the working electrode's potential with exceptional precision. Additionally, it possesses high sensitivity to detect very low currents, which is crucial in many advanced electrochemical studies.

Electrical measurements (Figure 3.10) were performed to calculate an approximation of "Vertical Resistance" using the potentiostat, specifically the "C-V linear potentiostatic function" on $PVA/Zn(NO_3)_2$ nanofibers obtained by electrospinning of the 4% solution, at different electrospinning times: 2 hours, 3 hours and 4 hours. The following parameters were used: Stabilization time of 15 seconds, Start and stop voltage of 0 V, First vertex voltage of 1 V, Second vertex voltage of -1 V, number of cycles of 1, and scan rate of 100 mV/s.
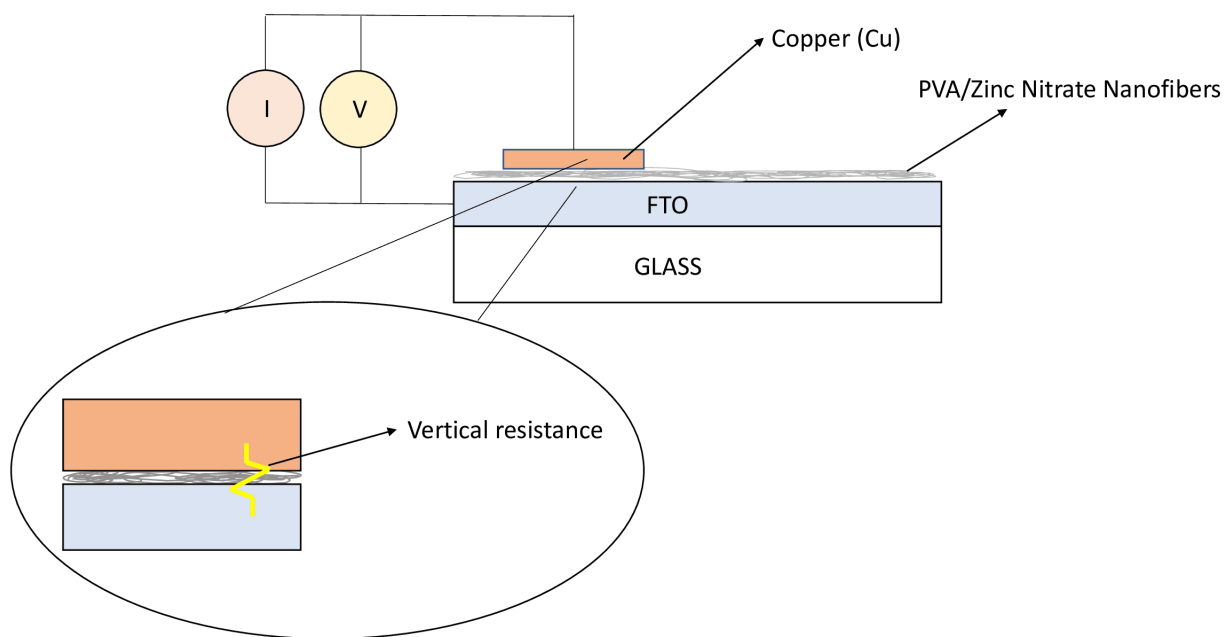
Figure 3.10: Measurement diagram in the potentiostat of current intensity vs. voltage using the "C-V linear potentiostatic function," where a voltage sweep is applied and the potentiostat measures the current flowing through the copper, the nanofiber layer, and the FTO substrate.

Chapter 4

Results & Discussion

4.1 Effects of calcination temperature on $PVA+Zn(NO_3)_2$ solution

4.1.1 Raman spectroscopy

Figures 4.1, 4.2, and 4.3 show the Raman spectra of 11% PVA + 10% $Zn(NO_3)_2$ solutions calcined at different temperatures, comparing them with the Raman spectrum of ZnO powder. In Figure 4.1, it is observed that the Raman spectrum of ZnO powder has specific peaks, such as 100, 332, and 438 cm^{-1}, indicating the characteristic vibrations of ZnO[69]. At 200 °C, the ZnO peaks are not observed as in the Raman spectrum of ZnO powder, suggesting that there is still no complete decomposition of PVA and zinc nitrate, and therefore no formation of ZnO at this calcination temperature. As the temperature increases to 300 °C, peaks such as 100 and 439 cm^{-1} become more prominent in the spectrum, and the overall intensity increases. This may indicate a greater interaction between PVA and zinc nitrate or the initial formation of ZnO[69]. At 400 °C, the intensity of the peaks such as 100 and 439 cm^{-1} is even higher in the spectrum, suggesting that a significant amount of ZnO is forming from the thermal decomposition of zinc nitrate at this temperature. The shape and location of the peaks may resemble those of the ZnO powder Raman spectrum, confirming the formation of ZnO[69]. Finally, in the spectra taken at different calcination temperatures, a gradual increase in intensity from approximately 1000 cm^{-1}

30

to 2000 cm^{-1} is observed, indicating fluorescence due to the intact presence of the PVA matrix or impurities.
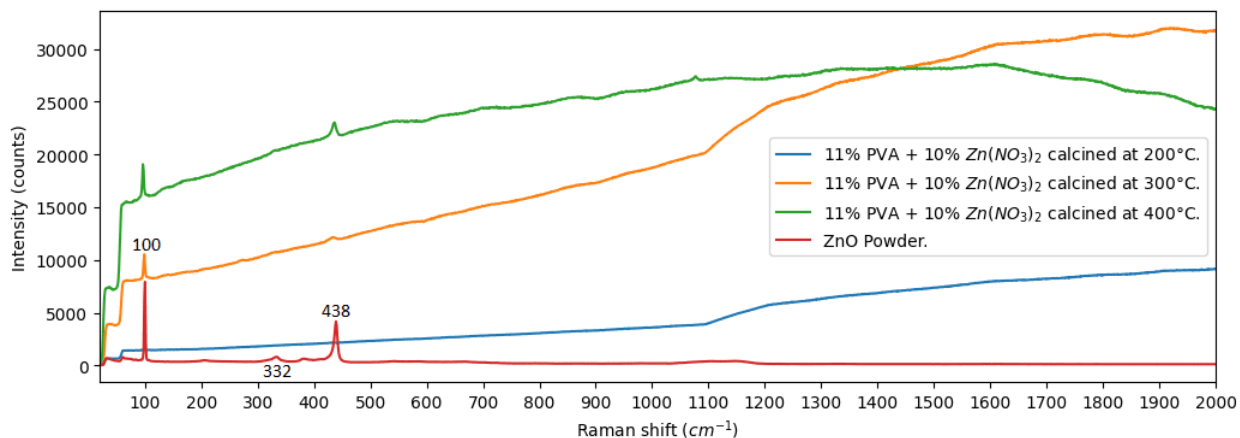
Figure 4.1: Raman spectroscopy results for calcination of zinc nitrate/polyvinyl alcohol solutions at 200 °C, 300 °C and 400 °C for 6 h.

In Figure 4.2, at 500 °C, a significant increase in the intensity of the 100, 332, and 438 cm^{-1} peaks is observed compared to the spectra at lower temperatures. This suggests considerable formation of ZnO from the decomposition of zinc nitrate. The similarity of the peaks to ZnO powder indicates effective formation of ZnO. At 600 °C, the peak intensity in this spectrum is slightly lower than in the 500 °C spectrum, which may indicate possible sintering or rearrangement of ZnO particles[70]. The presence of peaks similar to those in the ZnO powder Raman spectrum confirms that the material remains ZnO, but with possible variations in morphology or particle size[71]. At 700 °C, the intensity of the peaks decreases further, which could be due to an increase in the grain size of ZnO, reducing the specific surface area and, therefore, the Raman spectrum intensity. Despite this, the characteristic peaks of ZnO powder are present, confirming the stability of ZnO at this temperature[72]. Finally, the fluorescence effect is no longer observed in all spectra, suggesting the complete decomposition of PVA, but the presence of residual carbon, characterized by peaks at 1350 and 1600 cm^{-1}, is observed.
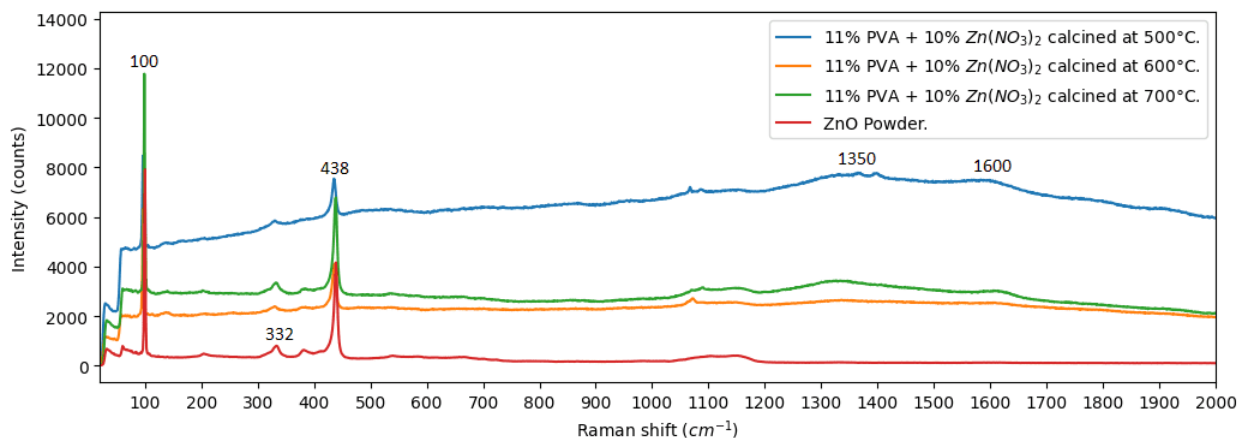
Figure 4.2: Raman spectroscopy results for calcination of zinc nitrate/polyvinyl alcohol solutions at 500 °C, 600 °C and 700 °C for 6 h.

In Figure 4.3, at 800 °C a significant increase in the intensity of the 100, 332, and 438 cm^{-1} peaks is observed compared to samples treated at lower temperatures. This suggests considerable formation of ZnO from the decomposition of zinc nitrate. The similarity of the peaks to the ZnO powder Raman spectrum indicates effective formation of ZnO. At 900 °C, the intensity of the peaks in this spectrum is higher than in the 800 °C spectrum, indicating a greater amount of ZnO formed at this temperature. The presence of characteristic peaks similar to those in the ZnO powder Raman spectrum confirms that the material remains ZnO. Finally, at 1000 °C, the intensity of the peaks slightly decreases compared to the 900 °C spectrum, which may be due to increased sintering and growth of ZnO particles[70]. Despite this, there are peaks similar to those in the ZnO powder Raman spectrum are present, confirming the stability of ZnO at this temperature. Finally, between 1100 and 1200 cm^{-1}, there is an elevation in each Raman spectrum of the calcined solution caused by the carbon formed during the calcination process. However, as the temperature increases, this elevation caused by the carbon decreases.
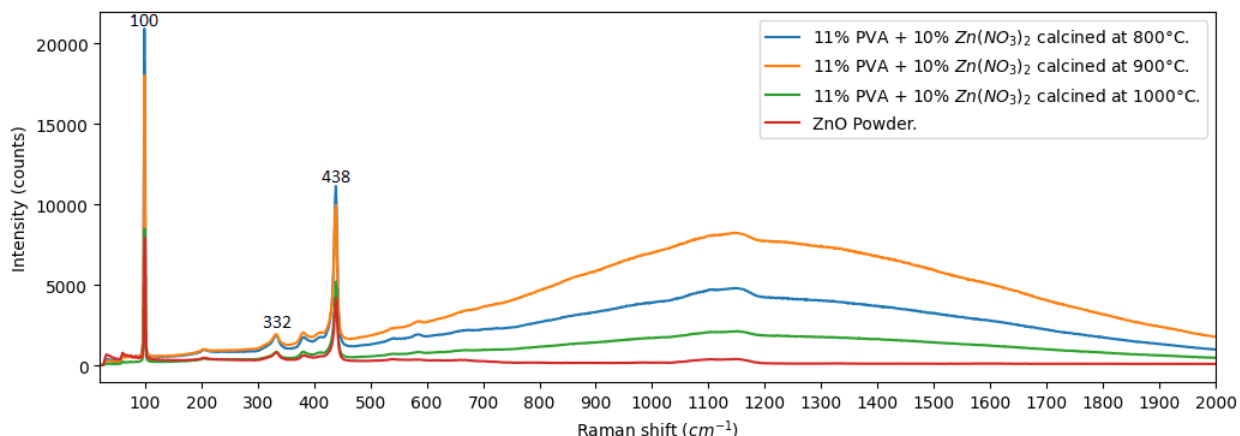
Figure 4.3: Raman spectroscopy results for calcination of zinc nitrate/polyvinyl alcohol solutions at 800 °C, 900 °C and 1000 °C for 6 h.

4.1.2   X-Ray Diffraction (XRD)

Figures 4.4, 4.5, and 4.6 show the XRD spectra of 11% PVA + 10% $Zn(NO_3)_2$ solutions calcined at different temperatures. In Figure 4.4, it can be observed that the XRD spectrum of ZnO powder has specific peaks at 31.7°, 34.4°, 36.2°, 47.5°, 56.6°, 62.8°, 67.9°, 68.5°, 72.5°, and 76.9°, which indicate the characteristic vibrations of zinc oxide[69]. At 200 °C, it is likely that zinc nitrate ($Zn(NO_3)_2$) begins to decompose partially, but the conversion to ZnO is not complete. The diffraction peaks in the spectrum of this sample are less intense and broader, indicating lower crystallinity and possible presence of intermediate phases[73]. At 300 °C, a greater part of the PVA and zinc nitrate decomposes, forming ZnO. The peaks in the spectrum of this sample are more intense and defined than at 200 °C, reflecting higher crystallinity of the formed ZnO. Peaks similar to those of the XRD spectrum of ZnO powder are observed, although they may be accompanied by some minor peaks of intermediate compounds or impurities[71]. At 400 °C, the decomposition of PVA and zinc nitrate is almost complete, resulting in the formation of ZnO. The peaks in the spectrum of this sample are even more intense and sharp, reflecting a well-defined crystalline structure of ZnO. Here the peaks of this spectrum closely align with the peaks of the XRD spectrum of ZnO powder[70].
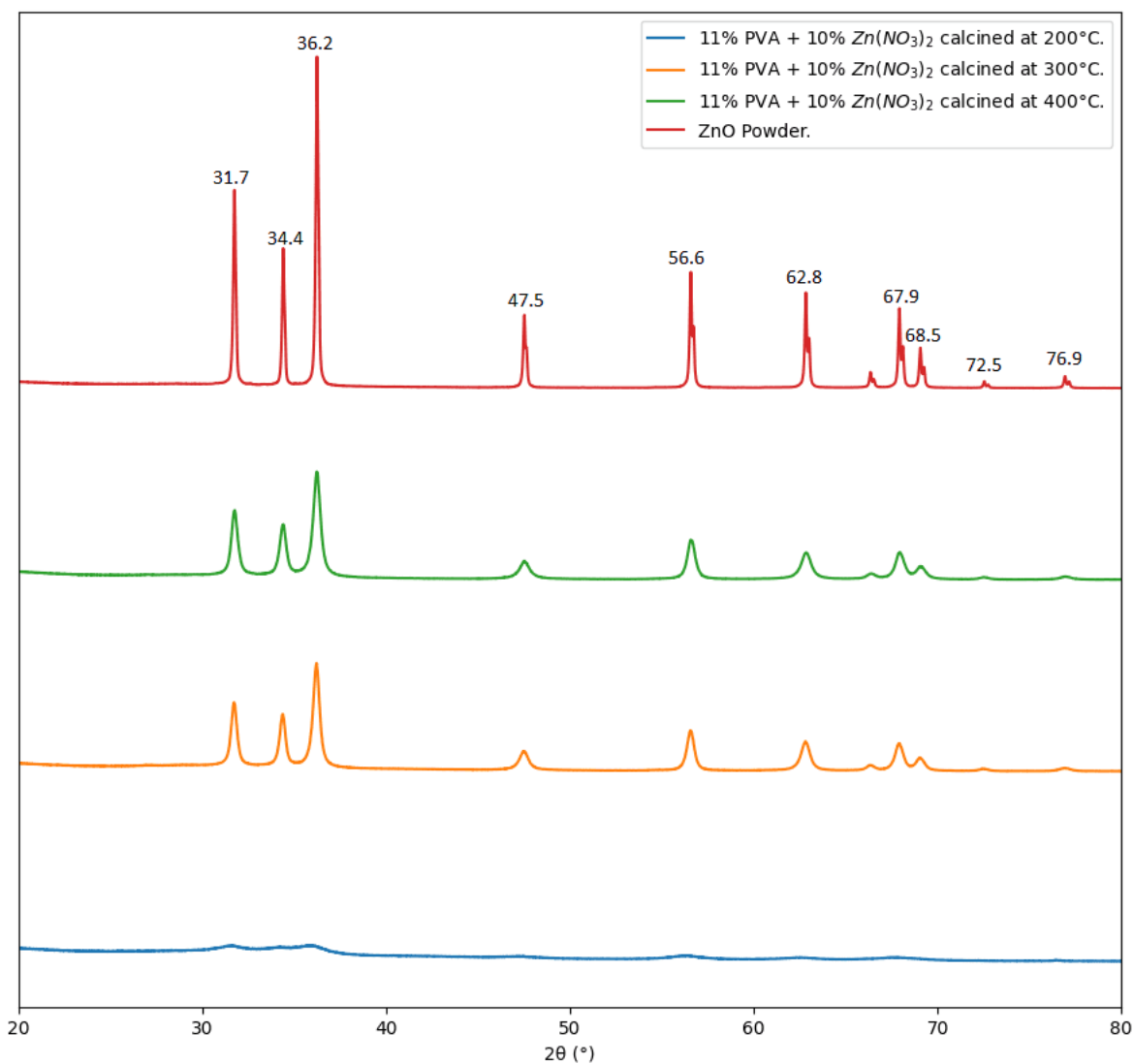
Figure 4.4: X-ray diffraction results for calcination of zinc nitrate/polyvinyl alcohol solutions at 200 °C, 300 °C and 400 °C for 6 h.

In Figure 4.5 at 500 °C, the formation of ZnO is evident, but the peaks are less intense compared to the XRD spectrum of ZnO powder. This suggests a relatively good conversion and crystallinity of $Zn(NO_3)_2$ to ZnO compared to the samples treated at lower temperatures[72]. At 600 °C, the peaks increase in intensity indicating greater conversion and crystallinity of ZnO.

The sample at 600 °C shows a more defined structure than at 500 °C[73]. The sample treated at 700 °C presents even more intense and defined peaks, approaching the intensity and definition of the XRD spectrum of ZnO powder. This suggests a complete conversion of $Zn(NO_3)_2$ to ZnO and high crystallinity[73].
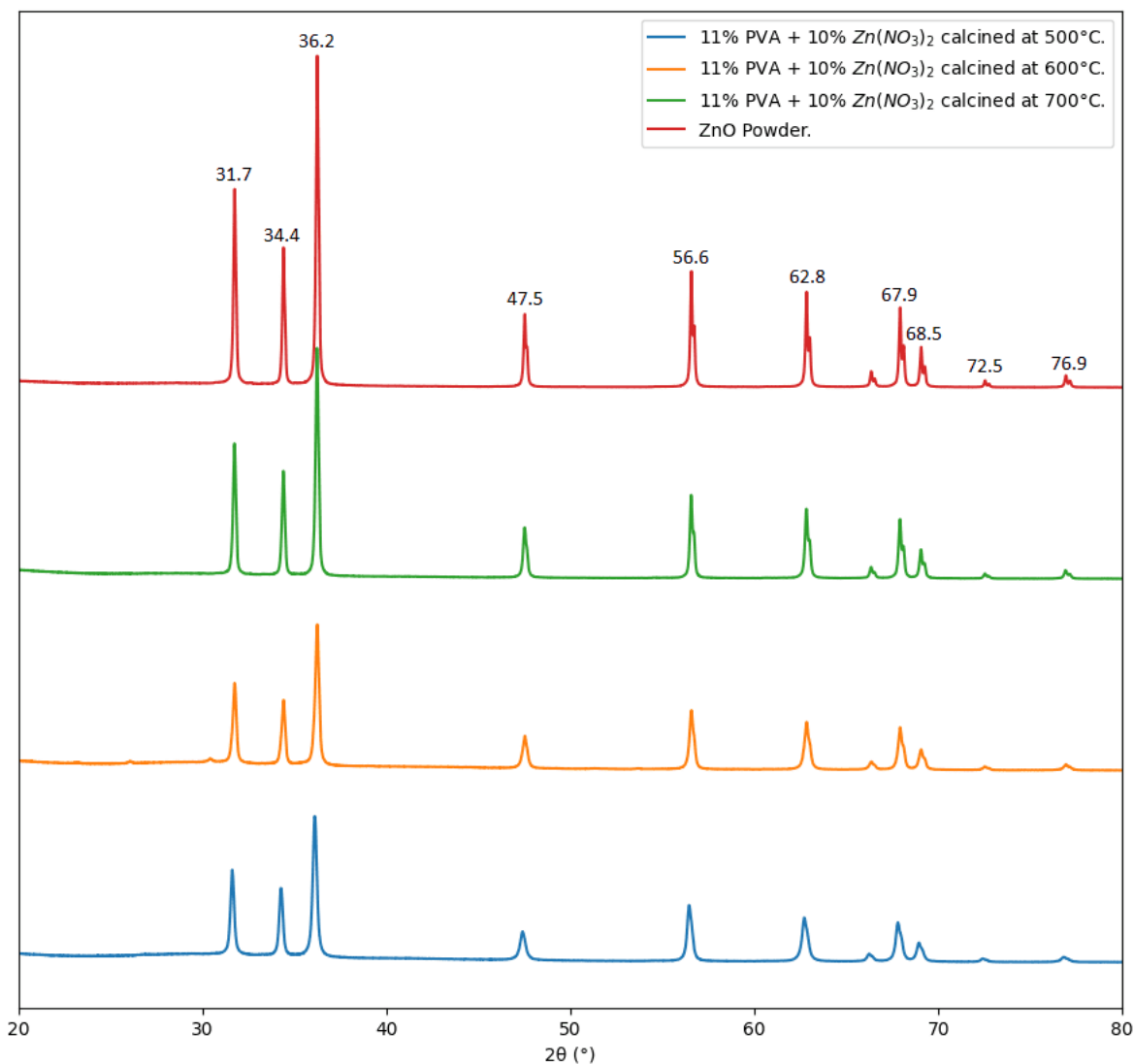
Figure 4.5: X-ray diffraction results for calcination of zinc nitrate/polyvinyl alcohol solutions at 500 °C, 600 °C and 700 °C for 6 h.

In Figure 4.6 at 800 °C, the decomposition of $Zn(NO_3)_2$ is complete, and the formation of ZnO crystals begins. Crystallization may not be as complete because the peaks in the XRD spectrum of this sample have lower intensity than the peaks in the XRD spectrum of ZnO powder. At 900 °C, the peaks are more intense and well-defined, unlike the peaks in the XRD spectrum of ZnO powder. The quality of the ZnO formed improved significantly[73]. The sample treated at 1000 °C presents peaks that reach intensities similar to those in the XRD spectrum of ZnO powder. Here, the formation of ZnO is optimal, with most impurities eliminated[73].
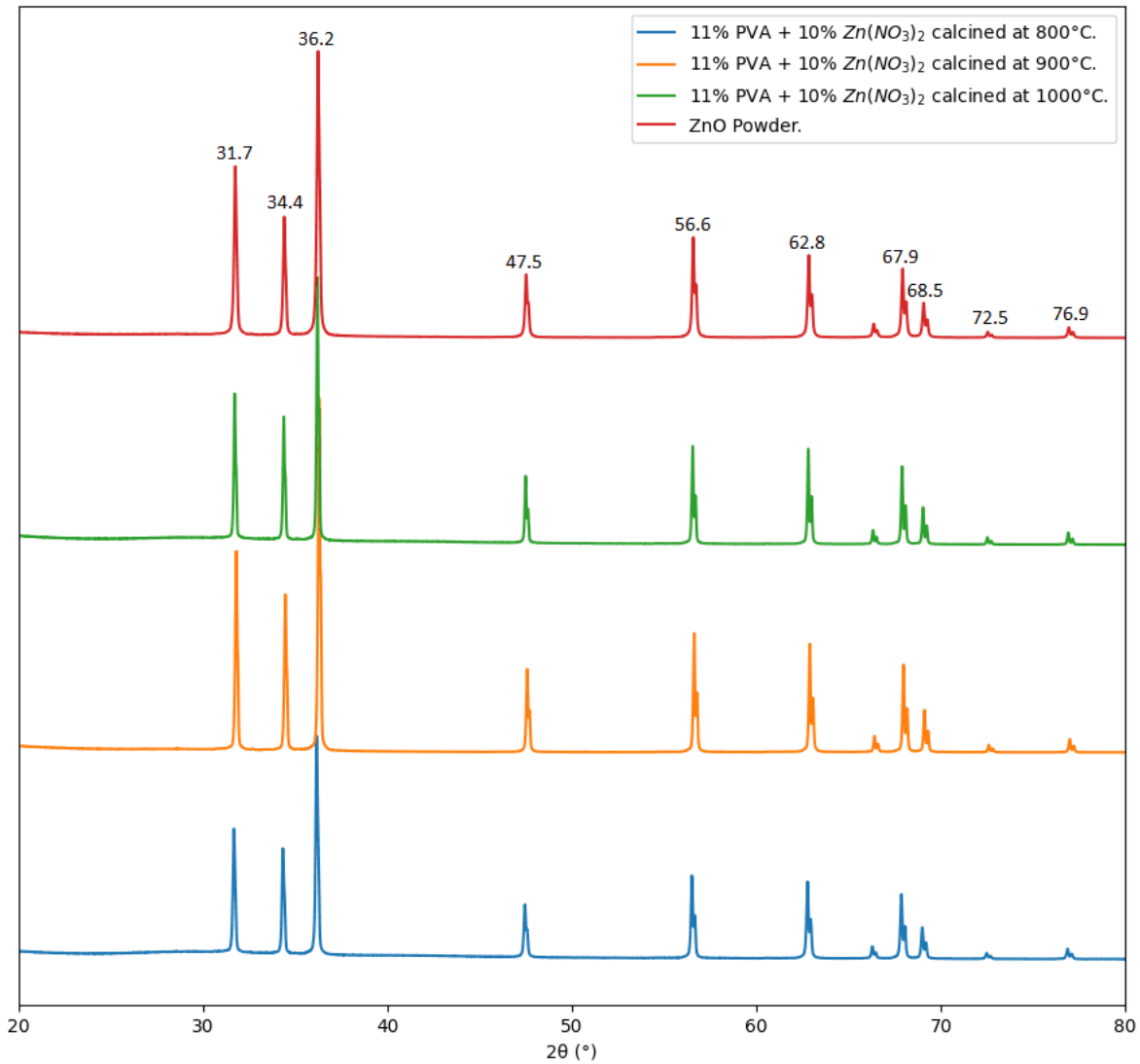
Figure 4.6: X-ray diffraction results for calcination of zinc nitrate/polyvinyl alcohol solutions at 800 °C, 900 °C and 1000 °C for 6 h.

Finally, after conducting this study on the formation of ZnO with these two characterizations, it has been determined that ZnO forms at 500 °C. Therefore, this temperature will be used for the calcination of PVA/Zinc Nitrate nanofibers for 6 hours to obtain ZnO nanofibers from now on.

4.2 Zn(NO$_3$)$_2$ concentration and Growth of nanofibers by electrospinning

Figure 4.9 (b) (4% solution) shows a fruitful formation of nanofibers before calcination compared to the 2% (Figure 4.9 (a)) and 6% (Figure 4.9 (c)) solutions. For the 6% solution, the high concentration of $Zn(NO_3)_2$ affects the surface tension, breaking bonds such as hydrogen bonds in the polymer structure and reducing viscosity, which does not allow us to have a stable Taylor cone, thus resulting in intermittent dripping (Figure 4.7 (b)). Meanwhile, for the 2% solution, the low concentration of $Zn(NO_3)_2$ may require additional parameter adjustments to achieve formation stability when used in electrospinning (Figure 4.7 (a)). Therefore, the 2% and 6% solutions result in limited nanofibers formation. Hence, due to the equilibrium and stability of the Taylor cone (Figure 4.10), we can determine that the 4% solution is optimal for nanofiber formation (Figure 4.8 (a)). On the other hand, the ZnO nanofibers obtained after calcination at 500°C for 6 hours still maintain their morphology and uniformity (Figure 4.8 (b)).
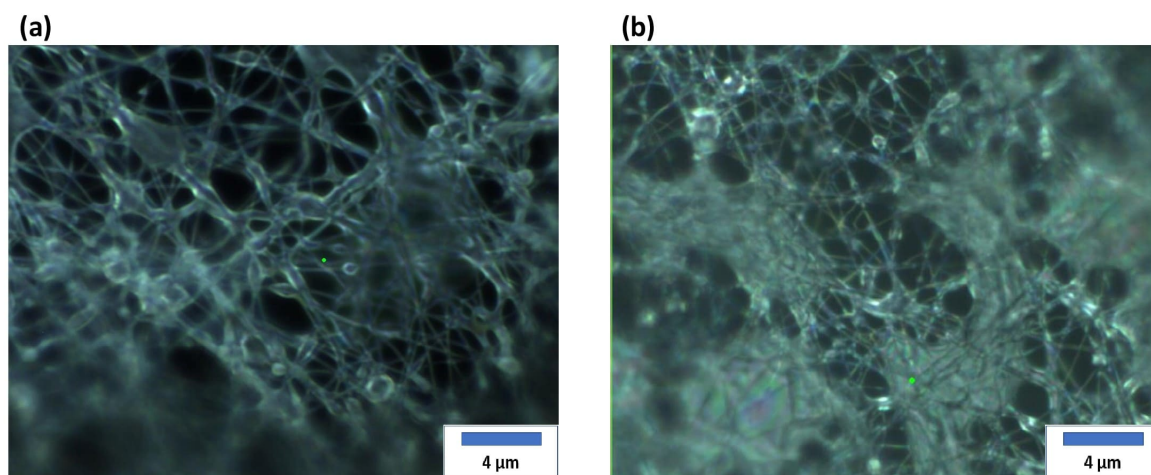
Figure 4.7: *PVA/Zn(NO$_3$)$_2$* nanofibers with intermittent drip: (a) 2% solution, and (b) 6% solution, all carried out with the same deposition time, observed from the optical microscope.
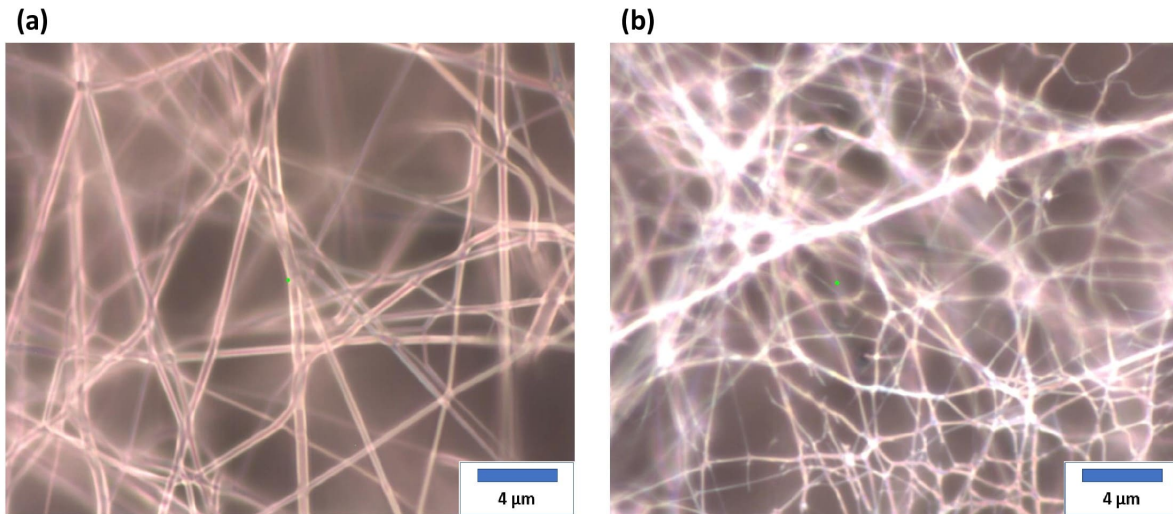
Figure 4.8: *PVA/Zn(NO$_3$)$_2$* nanofibers (4% solution): (a) uncalcined, and (b) calcined at 500°C for 6 hours (ZnO nanofibers), all carried out with the same deposition time, observed from the optical microscope.

Figures 4.11, 4.12, and 4.13 show nanofibers obtained from the 2%, 4%, and 6% solutions calcined for 6 hours at temperatures between 400 and 600°C, but their calcination was not good as it was done in the CVD furnace, and this caused the nanofibers to practically carbonize and take on a dark color when observed under the optical microscope. For this reason, the muffle furnace was chosen to carry out the calcination technique.
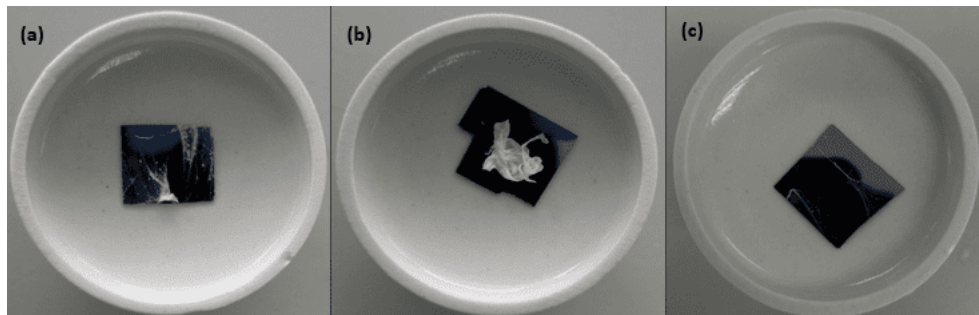
Figure 4.9: *PVA/Zn(NO$_3$)$_2$* nanofibers placed on Silicon substrates: (a) 2% solution, (b) 4% solution and 6% solution, all carried out with the same deposition time.
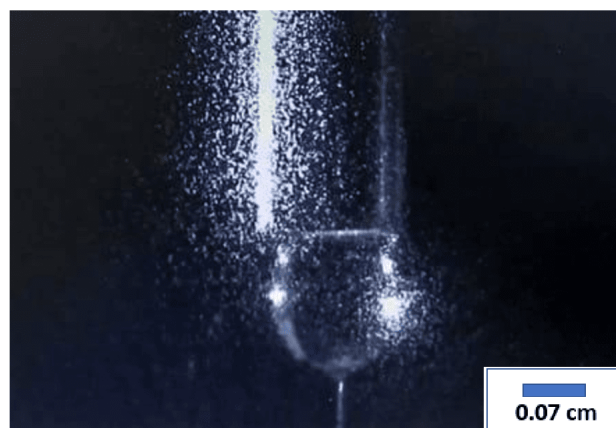
Figure 4.10: Taylor cone.
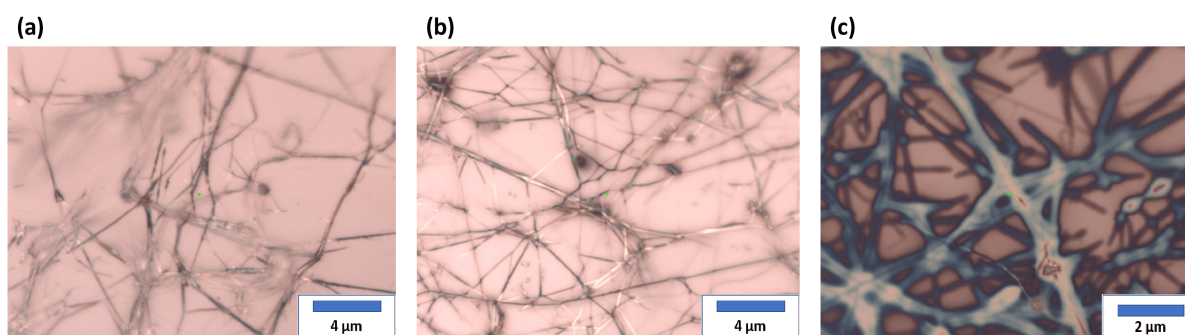
Figure 4.11: $PVA/Zn(NO_3)_2$ nanofibers (2% solution) calcined for 6h at: (a) 400°C, (b) 500°C, and (c) 600°C, observed from the optical microscope (first experimental attempt).
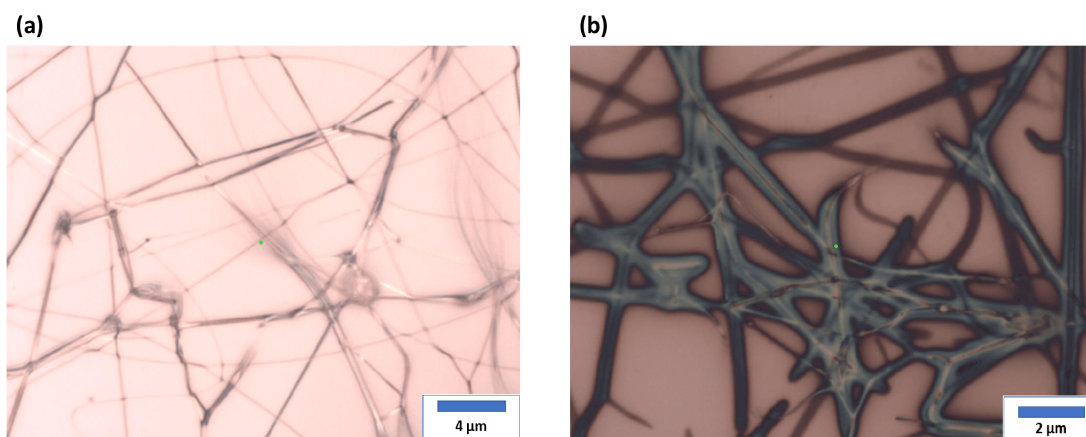
Figure 4.12: *PVA/Zn(NO₃)₂* nanofibers (4% solution) calcined for 6h at: (a) 400°C, and (b) 600°C, observed from the optical microscope (second experimental attempt).
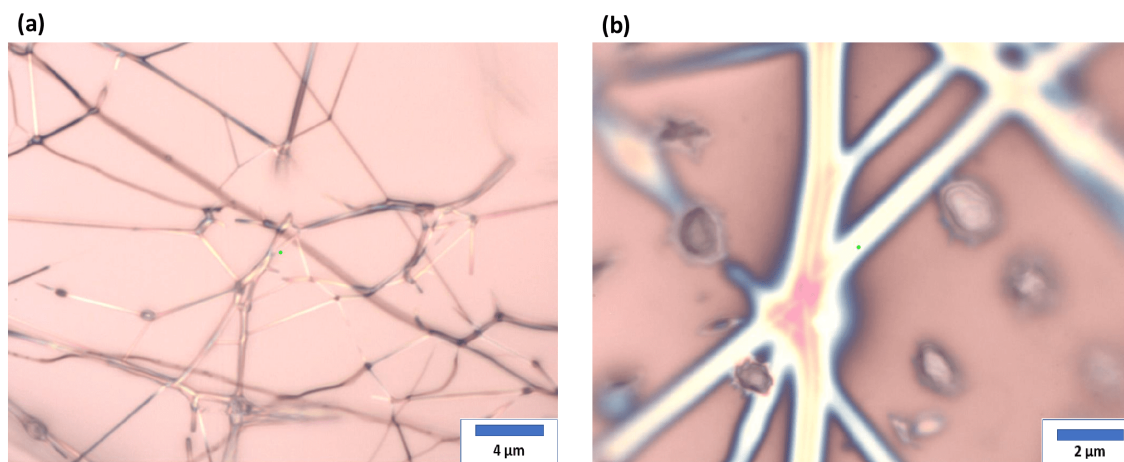
Figure 4.13: *PVA/Zn(NO₃)₂* nanofibers (6% solution) calcined for 6h at: (a) 400°C, and (b) 600°C, observed from the optical microscope (third experimental attempt).

4.2.1   Scanning electron microscopy (SEM)

The resulting morphological structure and chemical composition of the nanofibers obtained from the 2%, 4%, and 6% solutions after calcination produced zinc oxide nanofibers, which were

studied using SEM analysis. The SEM micrographs of zinc oxide (ZnO) nanofibers at different magnifications are presented in Figure 4.14. The ZnO nanofibers obtained of the 2% solution (Figure 4.14 (a)) show a less dense and more dispersed structure. Very fine and elongated nanofibers are observed, which are not very interwoven. The uniformity and diameter of the nanofibers appear to be variable, suggesting a very sparse formation process, possibly due to the low concentration of the solution. The nanofibers obtained from the 4% solution (Figure 4.14 (b)) are ZnO nanofibers begin to form a denser and more interwoven network. The nanofibers appear to be more uniformly distributed, and the diameter of the nanofibers may be more consistent. A greater number of nanofibers can be seen in the field of view compared to the nanofibers obtained from the 2% solution. In the 6% solution (Figure 4.14 (c)), the ZnO nanofibers obtained are very scarce, as the high concentration of $Zn(NO_3)_2$ affects the formation of nanofibers by altering the viscosity of the polymer (PVA). Additionally, it seems that the distance from the needle to the collector caused structural damage (broken nanofibers), unlike the nanofibers obtained from the 4% solution, which did not suffer damage at the same distance.
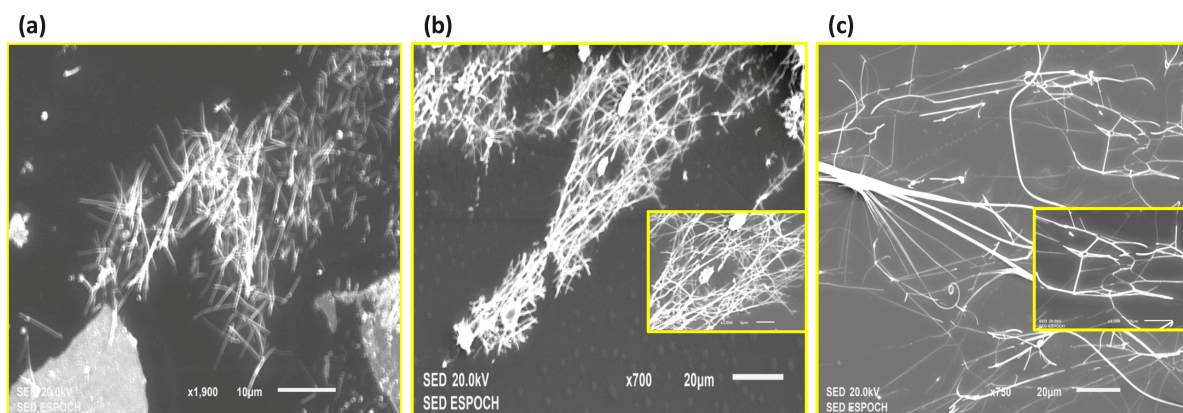
Figure 4.14: Scanning electron microscopy images of ZnO nanofibers obtained from calcining at 500°C for 6 hours the solutions: (a) 2% solution, (b) 4% solution (the inset image shows a zoom of the nanofibers) and (c) 6% solution (the inset image shows a zoom of the nanofibers).

4.2.2 Thermogravimetric Analysis (TGA)

The TGA test (Figure 4.15 (a) (green curve)) shows that the weight loss of pure PVA was completed in approximately 48 minutes at 500°C in air. There is a significant weight loss ($\approx$ 8%) around 200°C, which is generally attributed to the loss of adsorbed water from the PVA. A second significant weight loss ($\approx$ 73%) occurs between 200°C and 400°C, indicating the initial decomposition of PVA. A third significant weight loss ($\approx$ 18%) occurs between 400°C and 500°C, indicating the near-total decomposition of PVA. After 500°C, the curve stabilizes indicating that most of the material has decomposed. What remains is likely carbonaceous residue. The peaks in the derivative weight curve (Figure 4.15 (a) (blue curve)) correspond to the points of maximum weight loss rate. The peaks between 200°C and 500°C confirm the decomposition processes described earlier.

The TGA test (Figure 4.15 (b) (green curve)) demonstrates that the weight loss of the nanofibers obtained from the 4% solution was completed in approximately 40 minutes at 450°C in air[72]. There is a significant weight loss ($\approx$ 20%) around 200°C, which is generally attributed to the loss of adsorbed water and hydration water from the PVA and zinc nitrate. A second significant weight decrease ($\approx$ 45%) occurs between 200°C and 400°C, indicating the decomposition of PVA and the thermal decomposition of zinc nitrate to zinc oxide (ZnO). This stage corresponds to the decomposition of the organic material and the formation of the metal oxide[72]. After 400°C, the curve stabilizes, indicating that the remaining components of the sample are thermally stable up to 900°C. This suggests the presence of ZnO, which is known for its high thermal stability[72].

On the other hand, the peaks in the weight derivative (Figure 4.15 (b) (blue curve)) correspond to the points of maximum weight loss rate. The peak around 200°C and the peak between 300°C and 400°C confirm the decomposition processes described above. Finally, the decrease in nanofiber diameter over time may not have been caused by the decomposition of PVA and zinc nitrate. This may have been due to the contraction of ZnO by sintering[72].

Comparing the two TGA tests, it can be observed that both analyses begin with an initial weight loss around 100°C, corresponding to the removal of absorbed water. Both exhibit a major decomposition between 200°C and 400°C; in the case of pure *PVA*, this corresponds to a significant weight loss near 450°C, where the polymer begins to decompose completely, while for the *PVA/Zn(NO$_3$)$_2$* nanofibers, the drop is more gradual compared to pure *PVA*. This may be due to the decomposition of zinc nitrate, which could be catalyzing the decomposition of the

PVA. Finally, after 500°C for pure *PVA*, almost all the material has decomposed, leaving very little residue. In contrast, for the *PVA/Zn(NO₃)₂* nanofibers, after 500°C, a significant amount of residue remains, likely due to the formation of *ZnO* (zinc oxide), which is an inorganic material that does not decompose at these temperatures.
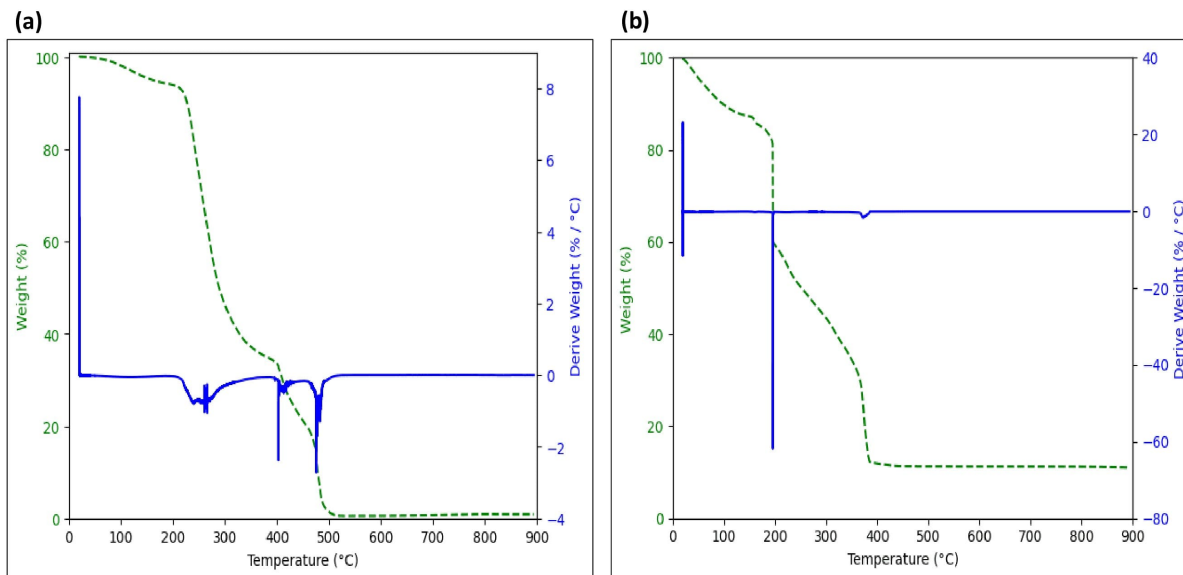
Figure 4.15: Typical thermogravimetric analysis-differential thermal analysis (TGA—DTA) curves of: (a) pure PVA, and (b) *PVA/Zn(NO₃)₂* nanofibers.

4.2.3 Atomic Force Microscopy (AFM)

The surface topography of *PVA/Zn(NO₃)₂* nanofibers was studied using non-contact atomic force microscopy. The 2D and 3D AFM images, recorded over a scanning area of 20 × 20 μm^2, are illustrated in Figure 4.16. In the 3D image, a fibrous structure is observed, not quite cylindrical due to the abundant accumulation of nanofibers. However, by manually measuring the diameter of some nanofibers, it can be seen that the diameters of the nanofibers range from 1500 to 2000 nm.

(a)

(b)
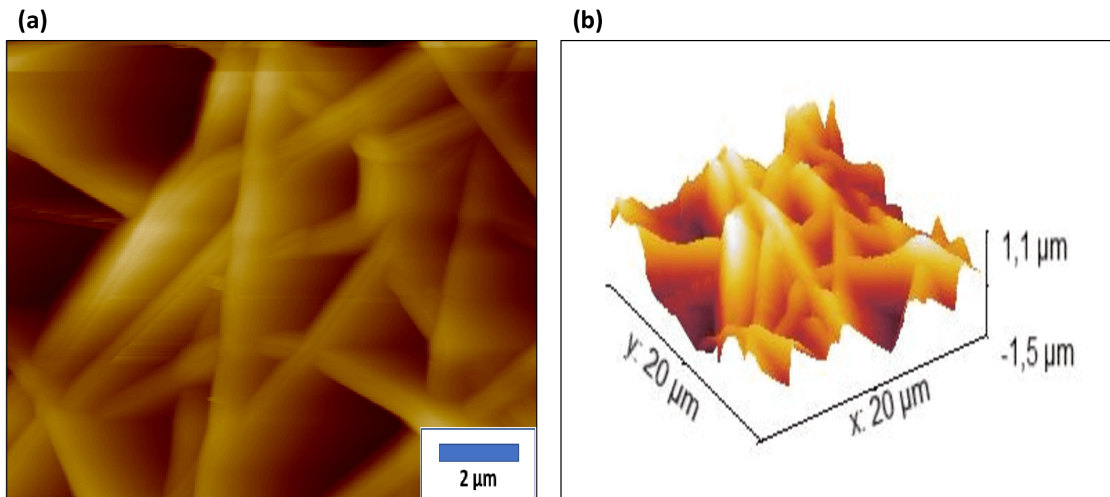
Figure 4.16: AFM of PVA / Zinc nitrate nanofibers before being calcined.

The surface topography of ZnO nanofibers was also studied using non-contact atomic force microscopy. The 2D and 3D AFM images, recorded over a scanning area of $20 \times 20 \ \mu m^2$, are illustrated in Figure 4.17. By manually measuring the diameter of some nanofibers, it can be seen that the diameters of the nanofibers range from 120 to 380 nm. It can be observed that the diameter of ZnO nanofibers after 6 hours of calcination was reduced by almost 90%, indicating that if the temperature and calcination time are increased, the diameter of the nanofibers will continue to decrease[48].
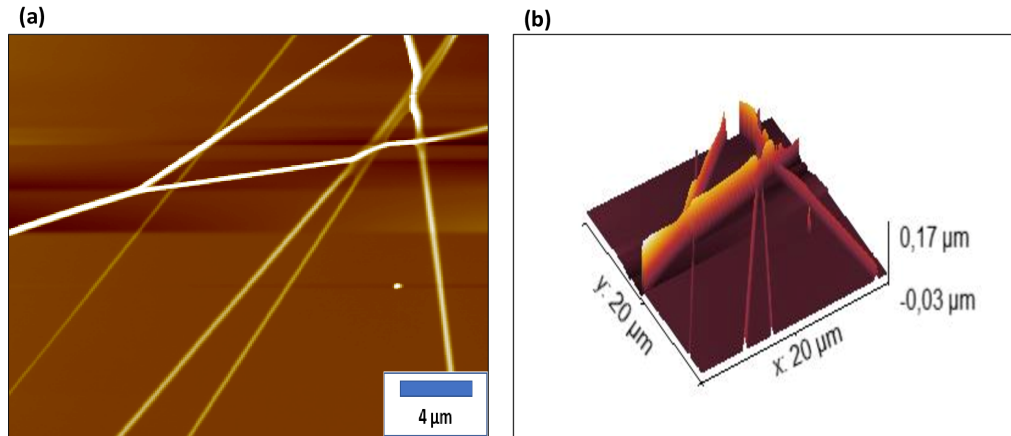
Figure 4.17: AFM of ZnO nanofibers.

In figure 4.18 (a), a phase change is observed in the $PVA/Zn(NO_3)_2$ nanofibers, where the white regions could indicate areas where the Zinc is more concentrated, while the dark regions may correspond to areas dominated by the PVA. In figure 4.18 (b), a phase change is observed in the ZnO nanofibers, where the white regions may represent areas with a concentration of ZnO, while the dark regions may correspond to areas with carbon residues originating from the calcination in the muffle furnace.
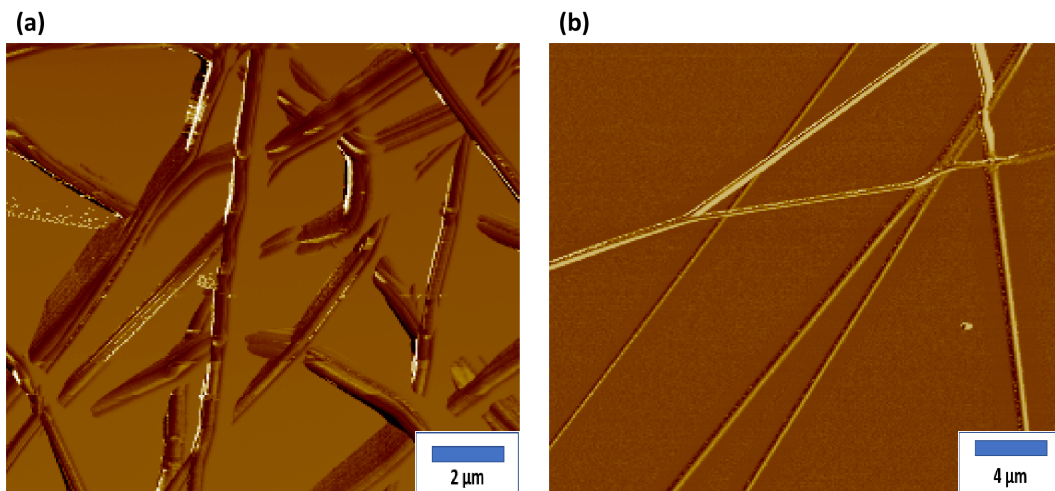
Figure 4.18: AFM of nanofiber phase: (a) $PVA/Zn(NO_3)_2$ and (b) ZnO

4.2.4 Fourier Transform Infrared Spectroscopy (FTIR)

Figure 4.19 (green curve (before calcination)) shows the FTIR spectrum of $PVA/Zn(NO_3)_2$ nanofibers obtained from the 4% solution. The spectrum shows characteristic peaks at 3300, 2900, 1640, 1400, 1310, and 1100 cm^{-1}, along with some clustered peaks between 750 and 950 cm^{-1}. The peak located at 3300 cm^{-1} is associated with the O-H stretching[74]. In PVA, this peak is typical due to the presence of hydroxyl groups (-OH) in its structure[74]. The peak located at 2900 cm^{-1} corresponds to the stretching of C-H bonds in the methylene group (-CH_2) of the PVA backbone[75]. This peak confirms the presence of the polymer. The peak around 1640 cm^{-1} could be related to the bending vibration of water molecules (H-O-H)[75]. It may also indicate the presence of a C=O stretching vibration, in case of slight oxidation or chemical interaction between the PVA and zinc nitrate. The peak located at 1400 cm^{-1} corresponds to the C-H bond deformation of PVA[76]. The peak at 1310 cm^{-1} is due to the presence of the nitrate group (NO_3^-) from zinc nitrate[76]. Nitrate typically shows bands in this region, specifically due to the asymmetric stretching of the N-O bonds. The peak near 1100 cm^{-1} is typical of the C-O stretching of PVA[74]. PVA contains C-O bonds that, along with O-H bonds, form its basic polyvinyl alcohol structure[75]. Finally, some clustered peaks between 750 and 950 cm^{-1} can be associated with the vibrations of the N-O bonds of zinc nitrate[76]. The signals between 750-950 cm^{-1} could also be related to PVA skeletal vibrations, as well as the interaction of Zn^+ with the polymer matrix[76]. This suggests that zinc has been incorporated into or interacts with the PVA nanofibers.

Figure 4.19 (red curve (after calcination)) shows the FTIR spectrum of ZnO nanofibers obtained from the calcination of $PVA/Zn(NO_3)_2$ nanofibers (4% solution) for 6 hours at 500 °C. The spectrum shows characteristic peaks at 700, 882, and 1358 cm^{-1}. The peak located at 700 cm^{-1} is characteristic of ZnO and is associated with the stretching of Zn-O bonds[77]. It is a clear indicator of the formation of zinc oxide after the calcination process. The strong absorption in this region is typical of ZnO-based materials[77]. The peak located at 882 cm^{-1} could be associated with residual C-C bonds from PVA that were not fully removed during calcination[76]. While the temperature of 500 °C is high enough to eliminate most organic compounds, traces of carbonaceous material or residues may remain. The peak located at 1358 cm^{-1} could be associated with residual nitrates (NO_3^-) not completely removed during calcination[76]. Nitrates tend to have bands in this region due to the asymmetric stretching vibrations of N-O bonds[76]. Finally, in the flat region from 2000 to 4000 cm^{-1}, the absence of significant peaks indicates that

most O-H (hydroxyl) and C-H (hydrocarbon) groups, typical of PVA, have been eliminated[76].
This confirms that the calcination process effectively decomposed the polymer matrix.
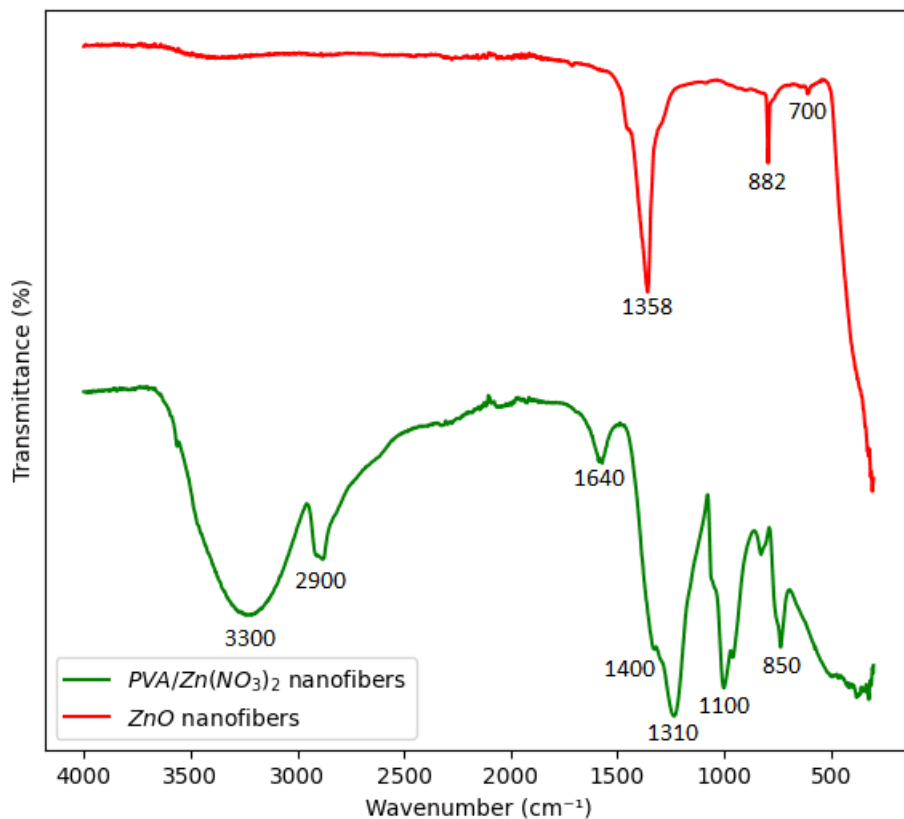
Figure 4.19: FTIR spectrum of: (a) *PVA/Zn(NO$_3$)$_2$* nanofibers, and (b) *ZnO* nanofibers.

4.2.5 Electrical Resistance Measurements

Electrical measurements on *PVA/Zn(NO$_3$)$_2$* nanofibers

Figure 4.20 shows the fitted curves of current intensity vs. voltage for uncalcined nanofibers
placed on FTO substrates at different electrospinning times (the average resistance was calculated
by performing 5 Current intensity-Voltage measurements with the potentiostat, along with its
corresponding error (Table 4.1)). The resistance that the nanofibers provide to the FTO was

calculated using the expression:

$$I = \frac{1}{R} \cdot V,$$

knowing that each line has the expression:

$$y = m \cdot x,$$

it follows that the slope of each line is equal to the inverse of the resistance, then:

$$\frac{1}{R} = m \rightarrow R = \frac{1}{m}$$
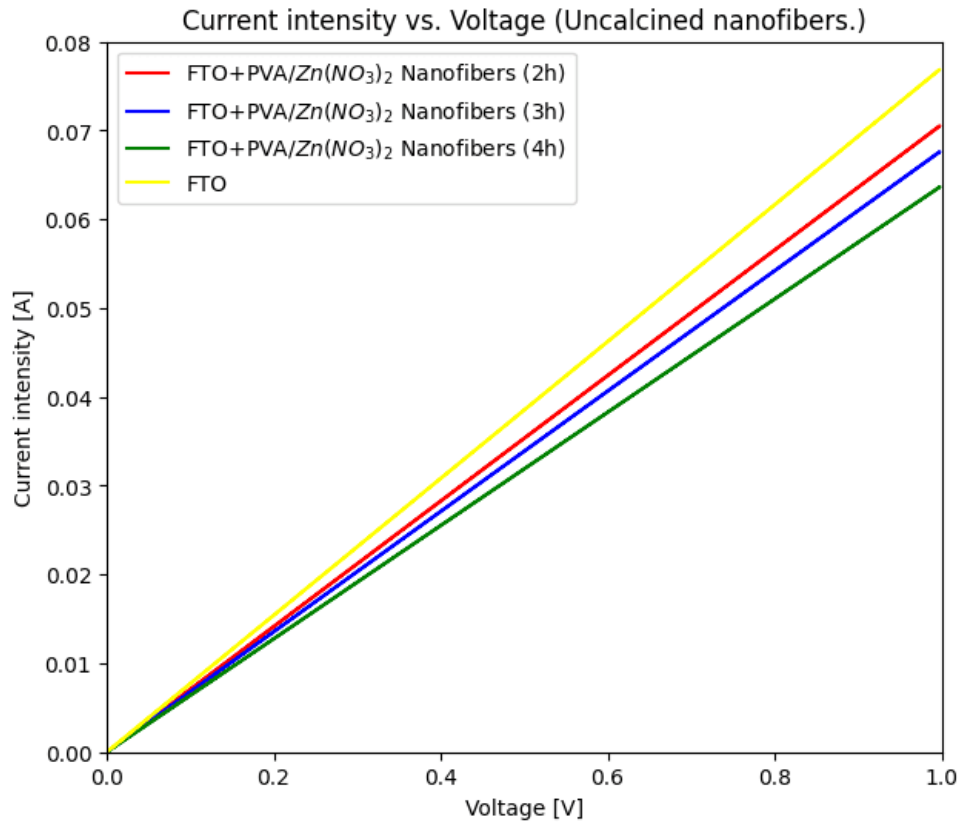
Figure 4.20: Current Intensity vs. Voltage of $PVA/Zn(NO_3)_2$ nanofibers placed on FTO substrates with different electrospinning times before being calcined.

The curve corresponding to the FTO substrate without nanofibers (yellow line) has a steeper slope, indicating lower resistance compared to the other curves of FTO substrates with $PVA/Zn(NO_3)_2$ nanofibers at different electrospinning times (red, blue, and green lines), which demonstrate that the inclusion of nanofibers increases the resistance of the FTO substrate, as the slopes of these curves are lower than that of the FTO substrate alone. As the electrospinning time increases, the thickness of the nanofiber layer on the FTO substrates also increases, and the slope of each FTO substrate curve with nanofibers decreases slightly, suggesting that the resistance increases with electrospinning time (Figure 4.25 (blue bars)), making the FTO substrates with nanofibers poor conductors. The Electrospinning process does not follow a specific order when depositing nanofibers on each substrate, which affects the thickness of the nanofiber layer, and therefore, can impact the calculation of each resistance. Additionally, performing each measurement with the Potentiostat generates an error for each calculated resistance (Table 4.1).

Electrospinning time (h)	Slope (A/V)	Resistance (Ω)	Measurement error
0	0.077	12.98	±0.001
2	0.071	14.15	±0.256
3	0.068	14.76	±0.393
4	0.064	15.68	±0.154

Table 4.1: Resistance of each FTO substrate with $PVA/Zn(NO_3)_2$ nanofibers at different electrospinning times before being calcined.

Electrical measurements on ZnO nanofibers

Figures 4.21, 4.22, and 4.23 show ZnO nanofibers with different electrospinning times placed on the FTO substrates, observed from the optical microscope.
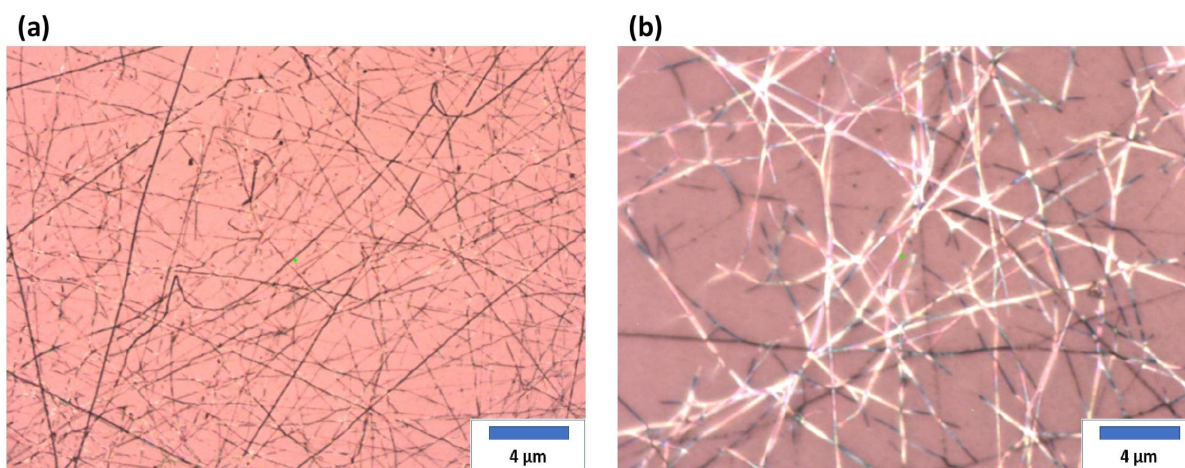
Figure 4.21: ZnO nanofibers with an electrospinning time of 2 hours observed with an objective of: (a) x20, and (b) x100.
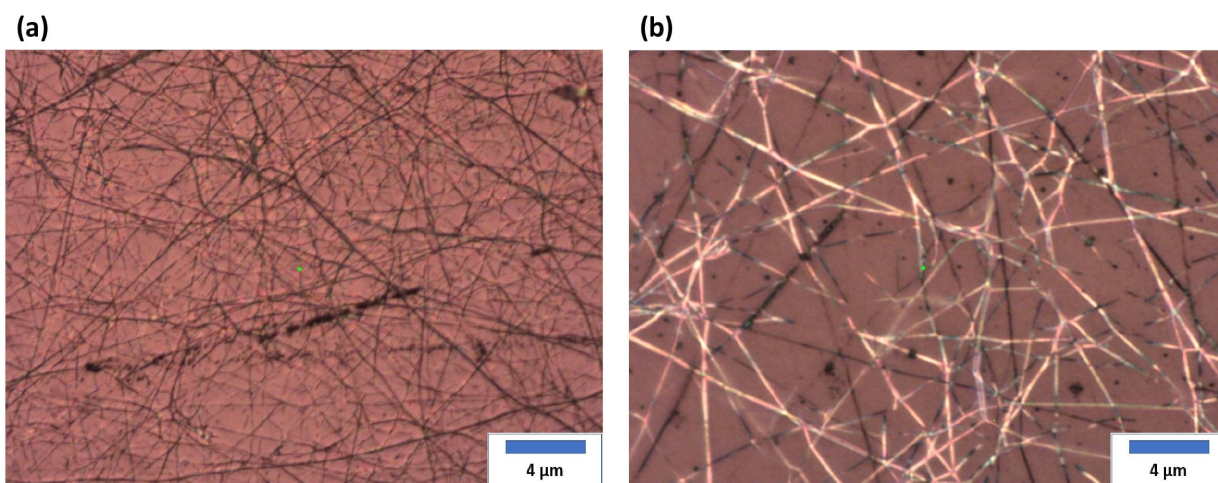
Figure 4.22: ZnO nanofibers with an electrospinning time of 3 hours observed with an objective of: (a) x20, and (b) x100.

(a)

(b)
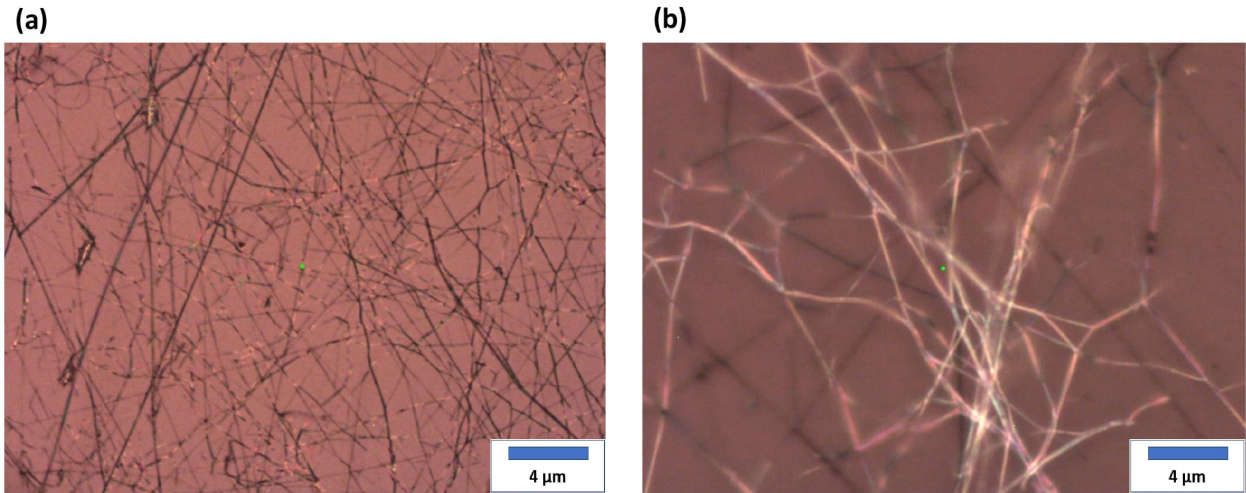
Figure 4.23: ZnO nanofibers with an electrospinning time of 4 hours observed with an objective of: (a) x20, and (b) x100.

Figure 4.24 shows the fitted lines of Current Intensity vs Voltage for ZnO nanofibers placed on FTO substrates, obtained from $PVA/Zn(NO_3)_2$ nanofibers with different electrospinning times, which were calcined for 6 hours at 500°C. The resistance that the ZnO nanofibers provide to the FTO substrate was calculated using the same procedure as for the uncalcined $PVA/Zn(NO_3)_2$ nanofibers (the average resistance was calculated by performing 5 Current intensity-Voltage measurements with the potentiostat, along with its corresponding error (Table 4.2)).
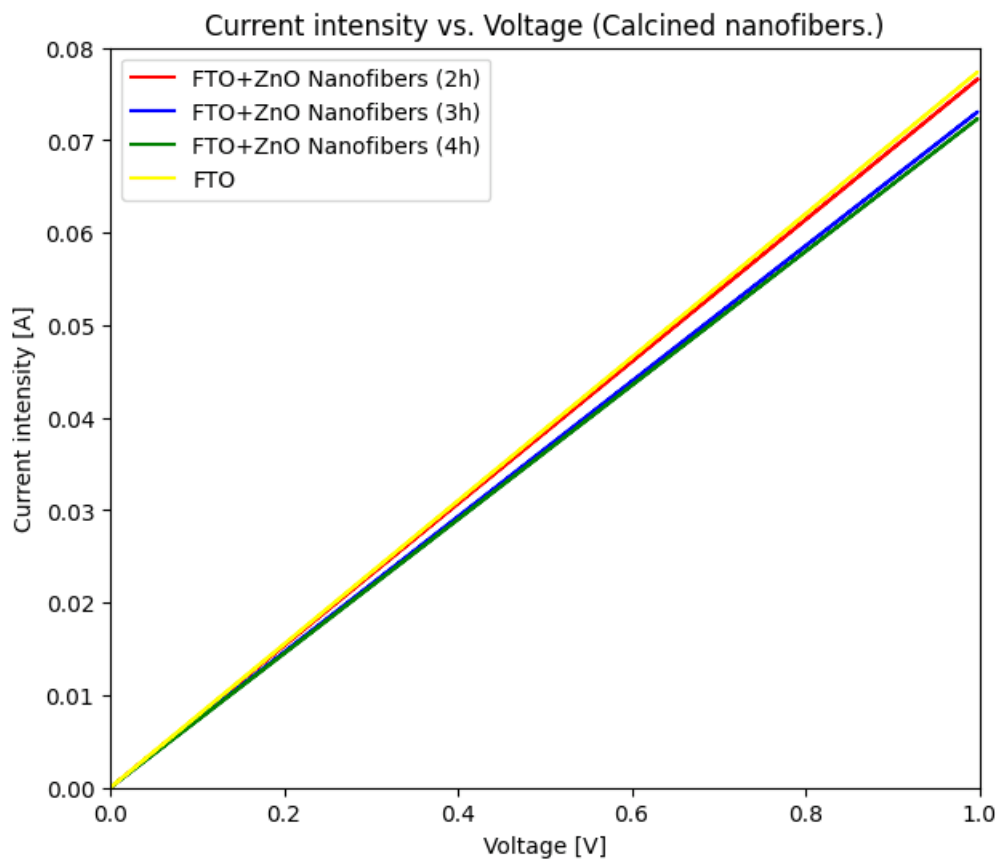
Figure 4.24: Current Intensity vs. Voltage of *ZnO* nanofibers placed on FTO substrates with different electrospinning times.

The curve of the FTO substrate without nanofibers (yellow line) has a steeper slope, indicating lower resistance compared to the other curves of FTO substrates with ZnO nanofibers at different electrospinning times (red, blue, and green lines). This shows that the inclusion of ZnO nanofibers slightly increases the resistance of the FTO substrate, as each slope of these curves is smaller than that of the bare FTO substrate. As the electrospinning time increases, the slope of each curve of the FTO substrate with ZnO nanofibers decreases minimally, but the thickness of the nanofiber layer also increases with electrospinning time, suggesting that the resistance increases with electrospinning time (Figure 4.25 (green bars)), making the FTO substrates with ZnO nanofibers poor conductors. The Electrospinning process does not follow a specific order when depositing

nanofibers on each substrate, which affects the thickness of the nanofiber layer, and therefore, can impact the calculation of each resistance. Additionally, performing each measurement with the Potentiostat introduces an error for each calculated resistance (Table 4.2).

Electrospinning time (h)	Slope (A/V)	Resistance (Ω)	Measurement error
0	0.077	12.98	±0.001
2	0.076	13.03	±0.166
3	0.073	13.66	±0.168
4	0.072	13.80	±0.124

Table 4.2: Resistance of each FTO substrate with ZnO nanofibers at different electrospinning times.
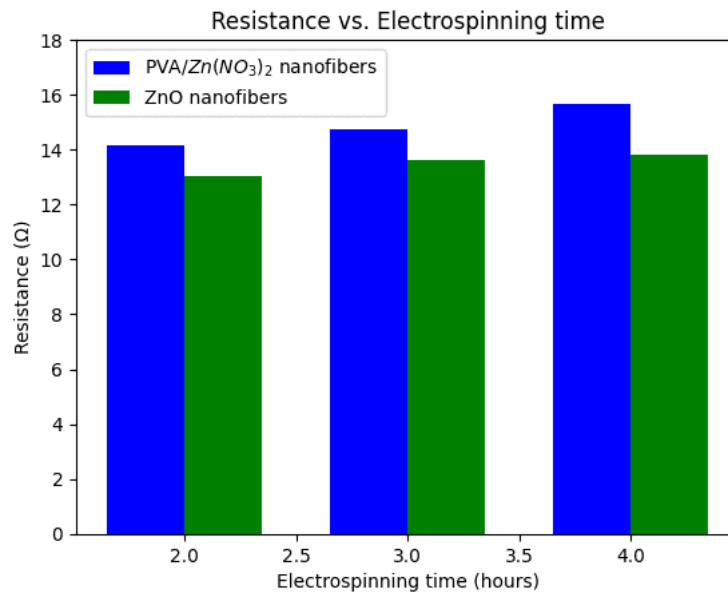
Figure 4.25: Bar diagram of the resistances obtained in the FTO substrates with nanofibers before (blue), and after calcination (green) at different electrospinning times.

Chapter 5

Conclusions

The present work reported the fabrication of electrospun nanofibers from a solution composed of 11% PVA and 4% Zinc Nitrate, which after applying calcination yielded ZnO nanofibers. The electrospinning technique is a relatively low-cost method that, with specific modifications, can be used for large-scale mass production. The method uses a high electric field to inject a polymer solution onto a collector, achieving polymerization and the formation of fibers on the micro or nanometric scale in the process. Raman spectroscopy analysis confirmed that the decomposition of PVA and Zinc Nitrate starts at 350°C, and the formation of Zinc Oxide occurs from 500°C with prominent peaks at 100, 332, and 438 cm^{-1}, which is consistent with the reviewed literature. Additionally, the X-ray diffraction analysis reveals a similarity in peaks intensity between the zinc oxide powder sample and the powder samples obtained from each calcination performed at 500°C and higher temperatures, from the 11% PVA and 10% Zinc Nitrate solution. The FTIR spectroscopy analysis showed peaks corresponding to functional groups and molecular structures of the $PVA/Zn(NO_3)_2$ nanofibers. It also allowed me to identify that after calcination, most functional groups of *PVA* were eliminated, leaving only some carbon and nitrate impurities, as well as peaks corresponding to *ZnO* in the *ZnO* nanofibers. On the other hand, the resulting SEM analysis showed that a solution of 11% PVA and 4% Zinc Nitrate (4% solution) is the ideal solution for nanofiber synthesis, as there was abundant nanofiber production and the diameter of the nanofibers was more consistent, unlike the 2% solution which shows a less dense and more dispersed structure, and the 6% solution shows scarce nanofiber formation due to the higher concentration of Zinc Nitrate which affects surface tension and hence

viscosity, impeding stable nanofiber formation. The resulting TGA test demonstrates that the weight loss of the nanofibers obtained from the 4% solution was completed in approximately 40 minutes at 450°C in air. The peak around 200°C indicates water loss, and the peak between 300°C and 400°C indicates the decomposition of PVA and $Zn(NO_3)_2$, and from 500°C the curve stabilizes indicating the formation of ZnO. On the other hand, the TGA test of pure PVA shows that the weight loss was completed in approximately 48 minutes at 500°C in air. The peak around 200°C indicates water loss, the peaks between 300°C and 400°C indicate the onset of PVA decomposition, the peaks between 400°C and 500°C indicate the near-total decomposition of PVA, and from 500°C the curve stabilizes indicating that most of the PVA has decomposed. AFM analysis helped us calculate the range of diameters of the $PVA/Zn(NO_3)_2$ nanofibers before calcination; these nanofibers had a range between 1500 and 2000 nm, but the ZnO nanofibers obtained after 6 hours of calcination reduced their diameter by almost 90%, with a range between 120 and 380 nm. Additionally, AFM analysis revealed a phase change in the $PVA/Zn(NO_3)_2$ nanofibers. The white regions likely indicate areas where Zinc is concentrated, while the dark regions correspond to areas dominated by PVA. The phase change observed in the ZnO nanofibers shows white regions that may represent areas with ZnO concentration, and dark regions that likely correspond to areas with carbon residues resulting from calcination in the muffle furnace. Finally, the calculated resistance in FTO substrates with $PVA/Zn(NO_3)_2$ nanofibers without calcination seems to increase as the electrospinning time increases, resulting in a decrease in the conductivity of the FTO substrates. Similarly, the calculated resistance in FTO substrates with ZnO nanofibers obtained after calcination also increases as the electrospinning time increases, leading to a thicker nanofiber layer, and consequently, a decrease in the conductivity of the FTO substrates.

Bibliography

[1] Lee, S.; Kim, S.; Shin, S.; Jin, Z.; Min, Y.-S. Band structure of amorphous zinc tin oxide thin films deposited by atomic layer deposition. *Journal of industrial and engineering chemistry* **2018**, *58*, 328–333.

[2] WHO, Air pollution. *World Health Organization (WHO)* **2021**,

[3] Gu, D.; Schüth, F. Synthesis of non-siliceous mesoporous oxides. *Chemical Society Reviews* **2014**, *43*, 313–344.

[4] Kang, Y.; Yu, F.; Zhang, L.; Wang, W.; Chen, L.; Li, Y. Review of ZnO-based nanomaterials in gas sensors. *Solid State Ionics* **2021**, *360*, 115544.

[5] Huang, Z.-M.; Zhang, Y.-Z.; Kotaki, M.; Ramakrishna, S. A review on polymer nanofibers by electrospinning and their applications in nanocomposites. *Composites science and technology* **2003**, *63*, 2223–2253.

[6] Park, J.-A.; Moon, J.; Lee, S.-J.; Lim, S.-C.; Zyung, T. Fabrication and characterization of ZnO nanofibers by electrospinning. *Current Applied Physics* **2009**, *9*, S210–S212.

[7] Blachowicz, T.; Ehrmann, A. Recent developments in electrospun ZnO nanofibers: A short review. *Journal of Engineered Fibers and Fabrics* **2020**, *15*, 1558925019899682.

[8] Di Mauro, A.; Zimbone, M.; Fragalà, M. E.; Impellizzeri, G. Synthesis of ZnO nanofibers by the electrospinning process. *Materials Science in Semiconductor Processing* **2016**, *42*, 98–101.

[9] Wang, Z. L. Zinc oxide nanostructures: growth, properties and applications. *Journal of physics: condensed matter* **2004**, *16*, R829.

[10] Li, D.; Xia, Y. Electrospinning of nanofibers: reinventing the wheel? *Advanced materials* **2004**, *16*, 1151–1170.

[11] Pérez, A. J. Semiconductores.¿ qué son y por qué son importantes? *Cuadernos Fronterizos* **2023**, 22–24.

[12] Prat Viñas, L.; Calderer Cardona, J. Dispositivos electrónicos y fotónicos: fundamentos. 2021.

[13] Rudan, M. *Physics of semiconductor devices*; Springer, 2015.

[14] Farrera, I. Conductores semiconductores y aislantes. *Universidad Autónoma. México. Recuperado de: http://depa. fquim. unam. mx/amyd/archivero/_27503. pdf* **2008**,

[15] Rashid, M. H. *Electrónica de potencia: circuitos, dispositivos y aplicaciones*; Pearson Educación, 2004.

[16] Linder, S. Semiconductores de potencia. Primera parte: bases y aplicaciones. *Revista ABB* **2006**, 34–39.

[17] Barras, A. M. Aplicación de óxidos semiconductores nanoestructurados (TiO2 y Ag-TiO2) como aditivo en el proceso germinativo de alfalfa. *Revista ABB* **2024**,

[18] Colinge, J.-P.; Colinge, C. A. *Physics of semiconductor devices*; Springer Science & Business Media, 2005.

[19] Peter, Y.; Cardona, M. *Fundamentals of semiconductors: physics and materials properties*; Springer Science & Business Media, 2010.

[20] Henini, M. Principles of Electronic Materials and Devices -SO Kasap: McGraw-Hill, 2002. 745 pp, ISBN 0-07-112237-0. *Microelectronics journal* **2002**, *33*, 681–681.

[21] Scholz, F. *Compound semiconductors: physics, technology, and device concepts*; Jenny Stanford Publishing, 2017.

[22] Streetman, B. G.; Banerjee, S. *Solid state electronic devices*; Prentice hall New Jersey, 2000; Vol. 4.

[23] Walia, S.; Balendhran, S.; Nili, H.; Zhuiykov, S.; Rosengarten, G.; Wang, Q. H.; Bhaskaran, M.; Sriram, S.; Strano, M. S.; Kalantar-zadeh, K. Transition metal oxides–Thermoelectric properties. *Progress in Materials Science* **2013**, *58*, 1443–1489.

[24] Lany, S. Semiconducting transition metal oxides. *Journal of Physics: Condensed Matter* **2015**, *27*, 283203.

[25] Cabero Piris, M. Fenómenos interfacionales asociados a vacantes de oxígeno en heteroestructuras de óxidos. *Revista ABB* **2018**,

[26] Wang, Z.-l.; Kang, Z. C. *Functional and smart materials: structural evolution and structure analysis*; Springer Science & Business Media, 2012.

[27] Diebold, U. The surface science of titanium dioxide. *Surface science reports* **2003**, *48*, 53–229.

[28] Ishigaki, T.; Yamauchi, S.; Kishio, K.; Mizusaki, J.; Fueki, K. Diffusion of oxide ion vacancies in perovskite-type oxides. *Journal of Solid State Chemistry* **1988**, *73*, 179–187.

[29] Kröger, F.; Vink, H. *Solid state physics*; Elsevier, 1956; Vol. 3; pp 307–435.

[30] Tang, Z.; Wong, G. K.; Yu, P.; Kawasaki, M.; Ohtomo, A.; Koinuma, H.; Segawa, Y. Room-temperature ultraviolet laser emission from self-assembled ZnO microcrystallite thin films. *Applied physics letters* **1998**, *72*, 3270–3272.

[31] Henderson, M. A. A surface science perspective on TiO2 photocatalysis. *Surface Science Reports* **2011**, *66*, 185–297.

[32] Look, D. C.; Reynolds, D.; Litton, C.; Jones, R.; Eason, D.; Cantwell, G. Characterization of homoepitaxial p-type ZnO grown by molecular beam epitaxy. *Applied physics letters* **2002**, *81*, 1830–1832.

[33] Taborda, J. A. P.; Gallego, J. L.; Roman, W. S.; Landázuri, H. R. Películas nano estructuradas de oxido de zinc (ZnO). *Scientia et technica* **2008**, *2*.

[34] Özgür, Ü.; Alivov, Y. I.; Liu, C.; Teke, A.; Reshchikov, M. A.; Doğan, S.; Avrutin, V.; Cho, S.-J.; Morkoç,; H, A comprehensive review of ZnO materials and devices. *Journal of applied physics* **2005**, *98*.

[35] Janotti, A.; Van de Walle, C. G. Oxygen vacancies in ZnO. *Applied Physics Letters* **2005**, *87*.

[36] Janotti, A.; Van de Walle, C. G. Fundamentals of zinc oxide as a semiconductor. *Reports on progress in physics* **2009**, *72*, 126501.

[37] Oba, F.; Togo, A.; Tanaka, I.; Paier, J.; Kresse, G. Defect energetics in ZnO: A hybrid Hartree-Fock density functional study. *Physical Review B—Condensed Matter and Materials Physics* **2008**, *77*, 245202.

[38] Vanheusden, K.; Seager, C.; Warren, W. t.; Tallant, D.; Voigt, J. Correlation between photoluminescence and oxygen vacancies in ZnO phosphors. *Applied physics letters* **1996**, *68*, 403–405.

[39] Korotcenkov, G. Metal oxides for solid-state gas sensors: What determines our choice? *Materials Science and Engineering: B* **2007**, *139*, 1–23.

[40] Look, D. C. Recent advances in ZnO materials and devices. *Materials science and engineering: B* **2001**, *80*, 383–387.

[41] Herrmann, J.-M. Heterogeneous photocatalysis: fundamentals and applications to the removal of various types of aqueous pollutants. *Catalysis today* **1999**, *53*, 115–129.

[42] Vasita, R.; Katti, D. S. Nanofibers and their applications in tissue engineering. *International Journal of nanomedicine* **2006**, *1*, 15–30.

[43] Li, W.-J.; Laurencin, C. T.; Caterson, E. J.; Tuan, R. S.; Ko, F. K. Electrospun nanofibrous structure: a novel scaffold for tissue engineering. *Journal of Biomedical Materials Research: An Official Journal of The Society for Biomaterials, The Japanese Society for Biomaterials, and The Australian Society for Biomaterials and the Korean Society for Biomaterials* **2002**, *60*, 613–621.

[44] Nayl, A. A.; Abd-Elhamid, A. I.; Awwad, N. S.; Abdelgawad, M. A.; Wu, J.; Mo, X.; Gomha, S. M.; Aly, A. A.; Bräse, S. Review of the recent advances in electrospun nanofibers applications in water purification. *Polymers* **2022**, *14*, 1594.

[45] Subbiah, T.; Bhat, G. S.; Tock, R. W.; Parameswaran, S.; Ramkumar, S. S. Electrospinning of nanofibers. *Journal of applied polymer science* **2005**, *96*, 557–569.

[46] Wang, X.; Dong, L.; Zhang, H.; Yu, R.; Pan, C.; Wang, Z. L. Recent progress in electronic skin. *Advanced Science* **2015**, *2*, 1500169.

[47] Lu, P.; Murray, S.; Zhu, M. *Electrospinning: Nanofabrication and Applications*; Elsevier, 2019; pp 695–717.

[48] Siddheswaran, R.; Sankar, R.; Ramesh Babu, M.; Rathnakumari, M.; Jayavel, R.; Murugakoothan, P.; Sureshkumar, P. Preparation and characterization of ZnO nanofibers by electrospinning. *Crystal Research and Technology: Journal of Experimental and Industrial Crystallography* **2006**, *41*, 446–449.

[49] Bhardwaj, N.; Kundu, S. C. Electrospinning: A fascinating fiber fabrication technique. *Biotechnology advances* **2010**, *28*, 325–347.

[50] Gallagher, P. K.; Brown, M. E. Handbook of thermal analysis and calorimetry. *Revista ABB* **2003**,

[51] Colthup, N. *Introduction to infrared and Raman spectroscopy*; Elsevier, 2012.

[52] Ferraro, J. R. *Introductory raman spectroscopy*; Elsevier, 2003.

[53] Mulvaney, S. P.; Keating, C. D. Raman spectroscopy. *Analytical Chemistry* **2000**, *72*, 145–158.

[54] Klug, H. P.; Alexander, L. E. *X-ray diffraction procedures: for polycrystalline and amorphous materials*; Elsevier, 1974.

[55] Robertson, J. Elements of X-ray diffraction by BD Cullity. 1979.

[56] Ermrich, M.; Opper, D. X-Ray powder diffraction. *XRD for the Analyst, Getting Acquainted with the Principles,* **2011**, 63–85.

[57] Goldstein, J. I.; Newbury, D. E.; Michael, J. R.; Ritchie, N. W.; Scott, J. H. J.; Joy, D. C. *Scanning electron microscopy and X-ray microanalysis*; springer, 2017.

[58] Wischnitzer, S. *Introduction to electron microscopy*; Elsevier, 2013.

[59] Lawes, G. Scanning electron microscopy and X-ray microanalysis. *Revista ABB* **1987**,

[60] Speyer, R. *Thermal analysis of materials*; CRC press, 1993.

[61] Wunderlich, B. *Thermal analysis of polymeric materials*; Springer Science & Business Media, 2005.

[62] Bevis, J.; Bottom, R.; Duncan, J.; Farhat, I.; Forrest, M.; Furniss, D.; MacNaughton, B.; Nazhat, S.; Saunders, M.; Seddon, A. *Principles and applications of thermal analysis*; Wiley Online Library, 2008.

[63] Binnig, G.; Quate, C. F.; Gerber, C. Atomic force microscope. *Physical review letters* **1986**, *56*, 930.

[64] Rugar, D.; Hansma, P. Atomic force microscopy. *Physics today* **1990**, *43*, 23–30.

[65] Stuart, B. H. *Infrared spectroscopy: fundamentals and applications*; John Wiley & Sons, 2004.

[66] Smith, B. C. *Fundamentals of Fourier transform infrared spectroscopy*; CRC press, 2011.

[67] Griffiths, P. R. Fourier transform infrared spectrometry. *Science* **1983**, *222*, 297–302.

[68] Bard, A. J.; Faulkner, L. R.; White, H. S. *Electrochemical methods: fundamentals and applications*; John Wiley & Sons, 2022.

[69] Garzón-Ramos, D.; Guzmán-Embús, D.; Serna-Plata, C.; Galvez-Coy, D.; Vargas-Hernández, C. Estudio de las propiedades estructurales, vibracionales y eléctricas de la matriz compleja PVA+ microvaras de ZnO. *Revista Colombiana de Materiales* **2014**, 250–256.

[70] Asadpour, S.; Kooravand, M.; Asfaram, A. A review on zinc oxide/poly (vinyl alcohol) nanocomposites: Synthesis, characterization and applications. *Journal of Cleaner Production* **2022**, *362*, 132297.

[71] Calleja, J.; Cardona, M. Resonant raman scattering in ZnO. *Physical Review B* **1977**, *16*, 3753.

[72] Wu, H.; Pan, W. Preparation of zinc oxide nanofibers by electrospinning. *Journal of the American Ceramic Society* **2006**, *89*, 699–701.

[73] Reddy, A. J.; Kokila, M.; Nagabhushana, H.; Rao, J.; Shivakumara, C.; Nagabhushana, B.; Chakradhar, R. Combustion synthesis, characterization and Raman studies of ZnO nanopowders. *Spectrochimica Acta Part A: Molecular and Biomolecular Spectroscopy* **2011**, *81*, 53–58.

[74] Sudhamani, S.; Prasad, M.; Sankar, K. U. DSC and FTIR studies on gellan and polyvinyl alcohol (PVA) blend films. *Food Hydrocolloids* **2003**, *17*, 245–250.

[75] Hema, M.; Selvasekarapandian, S.; Arunkumar, D.; Sakunthala, A.; Nithya, H. FTIR, XRD and ac impedance spectroscopic study on PVA based polymer electrolyte doped with NH4X (X= Cl, Br, I). *Journal of Non-Crystalline Solids* **2009**, *355*, 84–90.

[76] Norouzi, M. A.; Montazer, M.; Harifi, T.; Karimi, P. Flower buds like PVA/ZnO composite nanofibers assembly: Antibacterial, in vivo wound healing, cytotoxicity and histological studies. *Polymer testing* **2021**, *93*, 106914.

[77] de Peres, M. L.; Delucis, R. d. A.; Amico, S. C.; Gatto, D. A. Zinc oxide nanoparticles from microwave-assisted solvothermal process: Photocatalytic performance and use for wood protection against xylophagous fungus. *Nanomaterials and nanotechnology* **2019**, *9*, 1847980419876201.